DIFFUSION PRECONDITIONER FOR DISCONTINUOUS GALERKIN TRANSPORT PROBLEMS

A Thesis

by

ANTHONY PETRU BARBU

Submitted to the Office of Graduate Studies of
Texas A&M University
in partial fulfillment of the requirements for the degree of

MASTER OF SCIENCE

May 2011

Major Subject: Nuclear Engineering

DIFFUSION PRECONDITIONER FOR DISCONTINUOUS GALERKIN TRANSPORT PROBLEMS

A Thesis

by

ANTHONY PETRU BARBU

Submitted to the Office of Graduate Studies of
Texas A&M University
in partial fulfillment of the requirements for the degree of

MASTER OF SCIENCE

Approved by:

Chair of Committee,	Marvin L. Adams
Committee Members,	Jim E. Morel
	Vivek Sarin
Head of Department,	Raymond J. Juzaitis

May 2011

Major Subject: Nuclear Engineering

ABSTRACT

Diffusion Preconditioner for Discontinuous Galerkin Transport Problems.

(May 2011)

Anthony Petru Barbu, B.S., Texas A&M University

Chair of Advisory Committee: Dr. Marvin L. Adams

A simple Richardson iteration procedure converges slowly when applied to thick, diffusive problems with scattering ratios near unity. The current state of the art for overcoming this is to use a Krylov method with a diffusion preconditioner. However, the diffusion preconditioner must be tailored to the discretization of the transport operator to ensure effectiveness. We expand work from the bilinear discontinuous (BLD) finite element method (FEM) in two dimensions into a preconditioner applicable to all Discontinuous Galerkin FEMs in two and three dimensions. We demonstrate the effectiveness of our approach by applying it to the piecewise linear discontinuous (PWLD) FEM, which is notable for its flexibility with unstructured meshes. We employ a vertex-centered continuous FEM diffusion solution followed by local one-cell calculations to generate discontinuous solution corrections. Our goal is to achieve the same level of performance for PWLD and other methods, in two and three dimensions, as was previously achieved for BLD in two dimensions.

We perform a Fourier analysis of this preconditioner applied to the PWLD FEM and we test the preconditioner on a variety of test problems. The preconditioned Richardson method is found to perform well in both fine and coarse mesh limits; however, it degrades for high-aspect ratio cells. These properties are typical for partially consistent diffusion synthetic acceleration (DSA) schemes, and in particular they are exactly the properties of the method that was previously developed for BLD

in two dimensions. Thus, we have succeeded in our goal of generalizing the previous method to other Discontinuous Galerkin schemes.

We also explore the effectiveness of our preconditioner when used within the GMRES iteration scheme. We find that with GMRES there is very little degradation for cells with high aspect ratios or for problems with strong heterogeneities. Thus we find that our preconditioned GMRES method is efficient and effective for all problems that we have tested.

We have cast our diffusion operator entirely in terms of the single-cell matrices that are used by the discontinuous FEM transport method. This allows us to write our diffusion preconditioner without prior knowledge of the underlying FEM basis functions or cell shapes. As a result, a single software implementation of our preconditioner applies to a wide variety of transport options and there is no need to re-derive or re-implement a diffusion preconditioner when a new transport FEM is introduced.

To my wife and daughter, who kept me laughing, and helped write strange symbols

ACKNOWLEDGMENTS

I would like to thank Todd Wareing for laying the foundation for this research.

I would like to thank my committee Dr. Marvin Adams, Dr. Jim Morel, and Dr. Vivek Sarin, for their guidance and patience. Dr. Adams for his (near) infinite patience with students and brilliant ideas he's shared; Dr. Morel for his experience with diffusion accelerators, and their strengths and shortcomings; Dr. Sarin for his instructional class which led me to this area of research, and taught me everything I know about the Krylov methods which I've learned to love.

There are two individuals, Daryl Hawkins and Tim Smith, who have answered millions of programming questions for me. For this, I would like to thank them for their time and patience with a newbie to UNIX systems.

I also thank the Center for Large-scale Scientific Simulations (CLASS) and the Center for Radiative Shock Hydrodyamics (CRASH) for funding this research(er); hopefully this work will aid them in their goals.

TABLE OF CONTENTS

CHAPTER Page

LIST OF TABLES

LIST OF FIGURES

CHAPTER I

INTRODUCTION

A. Research Goals

The transport equation is used to describe many physical phenomena. When solving transport problems numerically, the angular dependence drastically increases the computational complexity. Acceleration schemes have been developed to hasten convergence in fewer iterations, of which the favored scheme in neutron and thermal radiation transport has been "diffusion-synthetic" acceleration, or DSA. These schemes, which we discuss in detail are lower order angular approximations of a transport operator. Research has shown DSA schemes derived consistently—in the same manner as the transport method by following a set procedure—have better convergence properties than arbitrarily chosen methods[1]. However, fully consistent schemes as described above can be computationally expensive: a coupled set of scalar flux and multidimensional current equations must be solved, and each equation has the same spatial degrees of freedom as the underlying transport discretization.

Our goal is to find a simplified procedure that maintains the behavior of fully consistent DSA schemes but reduces the computational complexity. The scheme derived will be tested with PWLD[2] finite elements, although it should be applicable to any finite element method. The target test platform is the PDT code at TAMU. This code is a multidisciplinary collaboration between the Nuclear Engineering and Computer Science departments which utilizes massively parallel algorithms. Currently

---

The journal model is *IEEE Transactions on Automatic Control.*

implemented is a multidimensional parallel transport solver for arbitrary polyhedral meshes. A Fourier analysis of the method will be performed to theoretically determine the properties of the preconditioned operator. The properties of the operator and the iterative performance with a Richardson iterative algorithm and with a Krylov iterative algorithm, specifically Generalized Minimum Residual (GMRES), will also be tested on a variety of problems using a code in MATLAB to do initial testing, and PDT to test larger problems, multigroup problems and 3D problems.

B. Problem Definition

We are interested in an operator split transport equation,

$$\begin{aligned} &\vec{\Omega}\cdot\vec{\nabla}\psi^{(l+1)}\left(\vec{r},\vec{\Omega},E\right)+\sigma_t\left(\vec{r},E\right)\psi^{(l+1)}\left(\vec{r},\vec{\Omega},E\right) \\ &=\int_{4\pi}d\Omega'\kappa\left(\vec{r},\vec{\Omega}',\vec{\Omega},E,E'\right)\psi^{(l)}\left(\vec{r},\vec{\Omega}',E\right)+Q\left(\vec{r},\vec{\Omega},E\right), \end{aligned} \tag{1.1}$$

where $\vec{\Omega}$ is the particle direction, E is the particle energy, $\vec{r}$ is the particle position, ψ is the particle angular intensity, l is the iteration step, σ_t is the total removal probability, κ is an arbitrary transfer operator from angle $\vec{\Omega}'$ to angle $\vec{\Omega}$ and energy E' to energy E, and Q is an arbitrary fixed source. We denote spatial vectors by an arrow (i.e. $\vec{x}$). We find iterates at half steps in anticipation of acceleration schemes which modify the iterate before setting it to the next whole step. We also define the following angle integrated quantity:

$$\phi=\int_{4\pi}\Omega'\psi\left(\vec{\Omega}\right). \tag{1.2}$$

The iteration procedure to solve Eq. (1.1) depends heavily on the transfer operator, κ (e.g. within-group scattering iterations, group-to-group scattering iterations, eigen-

value iterations, iterations on absorption rate density in thermal-radiation absorption-emission problems). Experience shows that preconditioners which are effective for within-group scattering iterations are also effective for other kinds of iterations. We therefore limit the scope of this research to the within-group scattering problem, isotropic scattering, and constant interaction probabilities within each discrete volume:

$$\begin{aligned} &\vec{\Omega} \cdot \vec{\nabla} \psi^{(l+1/2)} \left(\vec{r}, \vec{\Omega} \right) + \sigma_t \psi^{(l+1/2)} \left(\vec{r}, \vec{\Omega} \right) \\ &= \frac{\sigma_s}{4\pi} \int_{4\pi} d\Omega' \psi^{(l)} \left(\vec{r}, \vec{\Omega}' \right) + Q \left(\vec{r}, \vec{\Omega} \right), \end{aligned} \tag{1.3}$$

where σ_s is the isotropic scattering probability. We formulate the transport equation in weak (weighted-integral) form:

$$\begin{aligned} &\int_\tau d^3 r w\left(\vec{r}\right) \vec{\Omega} \cdot \vec{\nabla} \psi^{(l+1/2)} \left(\vec{r}, \vec{\Omega} \right) + \int_\tau d^3 r w\left(\vec{r}\right) \sigma_t \psi^{(l+1/2)} \left(\vec{r}, \vec{\Omega} \right) \\ &= \int_\tau d^3 r w\left(\vec{r}\right) \frac{\sigma_s}{4\pi} \int_{4\pi} d\Omega' \psi^{(l)} \left(\vec{r}, \vec{\Omega}' \right) + \int_\tau d^3 r w\left(\vec{r}\right) Q \left(\vec{r}, \vec{\Omega} \right), \end{aligned} \tag{1.4}$$

where $w\left(\vec{r}\right)$ is a weight function, and τ is a discrete volume of mesh. We use the divergence theorem twice on the weak form of the transport equation; the first application obtains quantities on surface $\partial\tau$ to couple the discontinuous problem to its neighbors:

$$\begin{aligned} &\int_{\partial\tau} d^2 r w\left(\vec{r}\right) \vec{n}\left(\vec{r}\right) \cdot \vec{\Omega} \psi_{\partial\tau}^{(l+1/2)} \left(\vec{r}, \vec{\Omega} \right) - \int_\tau d^3 r \vec{\nabla} w\left(\vec{r}\right) \cdot \vec{\Omega} \psi^{(l+1/2)} \left(\vec{r}, \vec{\Omega} \right) \\ &+ \int_\tau d^3 r w\left(\vec{r}\right) \sigma_t \psi^{(l+1/2)} \left(\vec{r}, \vec{\Omega} \right) \\ &= \int_\tau d^3 r w\left(\vec{r}\right) \frac{\sigma_s}{4\pi} \int_{4\pi} d\Omega' \psi^{(l)} \left(\vec{r}, \vec{\Omega}' \right) + \int_\tau d^3 r w\left(\vec{r}\right) Q \left(\vec{r}, \vec{\Omega} \right); \end{aligned} \tag{1.5}$$

the second application returns to a form which we may apply lumping easily, the weak form of the lumped transport equation:

$$\begin{aligned}
&\int_{\partial\tau} d^2rw\left(\vec{r}\right)\vec{n}\left(\vec{r}\right)\cdot\vec{\Omega}\left[\psi_{\partial\tau}^{(l+1/2)}\left(\vec{r},\vec{\Omega}\right)-\psi^{(l+1/2)}\left(\vec{r},\vec{\Omega}\right)\right]\\
&+\int_{\tau} d^3rw\left(\vec{r}\right)\vec{\Omega}\cdot\vec{\nabla}\psi^{(l+1/2)}\left(\vec{r},\vec{\Omega}\right)\\
&+\int_{\tau} d^3rw\left(\vec{r}\right)\sigma_t\psi^{(l+1/2)}\left(\vec{r},\vec{\Omega}\right)\\
&=\int_{\tau} d^3rw\left(\vec{r}\right)\frac{\sigma_s}{4\pi}\int_{4\pi} d\Omega'\psi^{(l)}\left(\vec{r},\vec{\Omega}'\right)+\int_{\tau} d^3rw\left(\vec{r}\right)Q\left(\vec{r},\vec{\Omega}\right).
\end{aligned} \tag{1.6}$$

C. Current State of the Problem

Early attempts to accelerate convergence of transport iterations using a lower order operator degraded, or even diverged, in certain limits. Alcouffe discovered that the low-order operator, if derived consistently with the transport operator, produced improved convergence properties in all limits (for certain problems) and used this discovery to create the first practical DSA methods. [3].

"Consistent" in this context means that the discrete diffusion operator is equivalent to the discrete transport operator given a low order approximation of angular variation. Larsen and McCoy developed a four-step procedure which ensures consistency of the low order with the transport discretization. A summary of the four-step procedure follows.

1. Define an additive correction to the latest iterate transport unknown as:

$$f\left(\vec{r},\vec{\Omega}\right)=\psi\left(\vec{r},\vec{\Omega}\right)-\psi^{(l+1/2)}\left(\vec{r},\vec{\Omega}\right). \tag{1.7}$$

   Subtract the iterative weak transport equation from the converged weak trans-

port equation to obtain an equation for this exact correction. Given a weighted-integral form of the transport equation with weight function w, the correction satisfies the weak form of the lumped transport correction equation:

$$\begin{aligned}
&\int_{\partial\tau} d^2r\vec{n}\left(\vec{r}\right)\cdot\vec{\Omega}w\left(\vec{r}\right)\left[f_{\partial\tau}\left(\vec{r},\vec{\Omega}\right)-f\left(\vec{r},\vec{\Omega}\right)\right]\\
&+\int_{\tau} d^3rw\left(\vec{r}\right)\vec{\Omega}\cdot\vec{\nabla}f\left(\vec{r},\vec{\Omega}\right)\\
&+\int_{\tau} d^3rw\left(\vec{r}\right)\sigma_t f\left(\vec{r},\vec{\Omega}\right)-\int_{\tau} d^3rw\left(\vec{r}\right)\frac{\sigma_s}{4\pi}\int_{4\pi} d\Omega' f\left(\vec{r},\vec{\Omega}'\right)\\
&=\int_{\tau} d^3rw\left(\vec{r}\right)\frac{\sigma_s}{4\pi}\left[\phi^{(l+1/2)}\left(\vec{r}\right)-\phi^{(l)}\left(\vec{r}\right)\right],
\end{aligned} \tag{1.8}$$

2. Make the P_1 approximation to the additive correction:

$$f\left(\vec{r},\vec{\Omega}\right)\approx\frac{1}{4\pi}\left[F\left(\vec{r}\right)+3\vec{\Omega}\cdot\vec{G}\left(\vec{r}\right)\right] \tag{1.9}$$

and take the 0^{th} and 1^{st} angular moments of the transport correction equation:

$$\begin{aligned}
&\int_{\partial\tau} d^2rw\left(\vec{r}\right)\vec{n}\left(\vec{r}\right)\cdot\int_{4\pi} d\Omega\,\vec{\Omega}\,\frac{1}{4\pi}\left[F_{\partial\tau}\left(\vec{r}\right)+3\vec{\Omega}\cdot\vec{G}_{\partial\tau}\left(\vec{r}\right)\right]\\
&-\int_{\partial\tau} d^2rw\left(\vec{r}\right)\vec{n}\left(\vec{r}\right)\cdot\vec{G}\left(\vec{r}\right)\\
&+\int_{\tau} d^3r\,w\left(\vec{r}\right)\vec{\nabla}\cdot\vec{G}\left(\vec{r}\right)+\int_{\tau} d^3r\,w\left(\vec{r}\right)\left[\sigma_t-\sigma_s\right]F\left(\vec{r}\right)\\
&=\int_{\tau} d^3r\,w\left(\vec{r}\right)\sigma_s\left[\phi^{(l+1/2)}\left(\vec{r}\right)-\phi^{(l)}\left(\vec{r}\right)\right]
\end{aligned} \tag{1.10}$$

$$\begin{aligned}
&\int_{\partial\tau} d^2r\vec{n}\left(\vec{r}\right)w\left(\vec{r}\right)\cdot\int_{4\pi} d\Omega\vec{\Omega}\vec{\Omega}\frac{1}{4\pi}\left[F_{\partial\tau}\left(\vec{r}\right)+3\vec{\Omega}\cdot\vec{G}_{\partial\tau}\left(\vec{r}\right)\right]\\
&-\int_{\partial\tau} d^2r\vec{n}\left(\vec{r}\right)w\left(\vec{r}\right)\frac{1}{3}F\left(\vec{r}\right)\\
&+\frac{1}{3}\int_{\tau} d^3rw\left(\vec{r}\right)\vec{\nabla}F\left(\vec{r}\right)+\int_{\tau} d^3r\,w\left(\vec{r}\right)\sigma_t\left(\vec{r}\right)\vec{G}\left(\vec{r}\right)=0
\end{aligned} \tag{1.11}$$

3. Eliminate the current corrections (the vector function $\vec{G}$) from Eq.(1.10), leaving a discrete diffusion-like equation for the scalar correction, F. For simple spatial discretization such as diamond differencing on orthogonal grids, the G unknowns can be algebraically eliminated a priori. However, given the spatial discretization that we are interested in, such as discontinuous FEM methods on structured or unstructured grids, this cannot be done, and one is left with a coupled system of equations for F, G_x, G_y, and (in 3D) G_z.

4. Use the low order scalar correction variable with the 0th moment of Eq.(1.9) to update the scalar variable:

$$\phi^{(l+1)}\left(\vec{r}\right) = \phi^{(l+1/2)}\left(\vec{r}\right) + F\left(\vec{r}\right) \tag{1.12}$$

Although the four-step method produces a very effective preconditioner, the inability to eliminate the current corrections in Step 3 has prevented this from being used for advanced spatial discretization such as those we consider in this work. The solution of the P1 system of equation has proved to be costly as each of these equations is coupled throughout the entire problem domain.

To avoid the high cost of solving this system of equations, researchers sought methods with reduced complexity but "enough consistency" to be effective. Some methods were created that behaved well despite not being strictly consistent in the P1 sense defined above. Wareing *et al.* devised a method in which the low-order diffusion operator was derived by taking the asymptotic diffusion limit of the bilinear discontinuous FEM (BLD) transport equation. This method performed well for fine and intermediate meshes but its performance degraded for optically thick cells. Wareing *et al.* later improved this by including a local post-diffusion calculation (in which

each cell's calculation is independent) to obtain discontinuous corrections from the continuous asymptotic diffusion equation.[4]

Wareing *et al.* described their method in two dimensions explicitly for BLD finite elements. In this thesis we begin with Wareing's 2D BLD method and extend it in several ways. First, we simplify the derivation of the low-order equation by defining rules that can be used to transform the fully consistent equations into equations much like those of Wareing *et al.* Second, we take advantage of our simplified derivation to generalize the method to arbitrary discontinuous FEMs (DFEMs) and arbitrary spatial grids. Third, we modify the stiffness (leakage) operator in the low-order equations in such a way that we can express the low-order operators entirely in terms of single-cell matrices that are already defined and used by the transport DFEM. This has considerable practical advantages – it allows the preconditioner coding to be written independent of the details of any particular DFEM or any particular kind of spatial grid.

D. Chapter Overview

In Chapter II we derive and compare several versions of low-order diffusion-based operators that can be used as preconditioners for DFEM transport iterations. These include an inconsistent operator that produces a continuous correction, a fully consistent operator from which the current corrections cannot be easily eliminated, and our proposed operator that is a generalization of the 2D BLD operator derived by Wareing, *et al.*[4]

Chapter III contains analysis of unaccelerated iteration, inconsistent DSA, and the

proposed method that uses Fourier expansion of iteration error modes. It includes spectral radii maps of the proposed operator with various parameters; parameters include aspect ratio of cells, scattering ratio, and optical thickness of each cell.

Chapter IV presents and discusses numerical results we have obtained using the new method. We discuss the additions made to the PDT code, describe the test problems, and present and discuss the results from the test problems.

Chapter V summarizes results, discusses conclusions we make about those results, and suggests avenues for future work.

CHAPTER II

METHOD DESCRIPTION

In this chapter we first introduce a finite element notation which will simplify the remaining equations, and apply them to equations introduced in the first chapter. Next we derive the fully consistent DSA method. We then derive an inconsistent DSA scheme which utilizes only transport matrices. Finally we derive the proposed method; the derivation includes a discussion of approximations made during the derivation and the appropriateness of each approximation.

We remind the reader that we have simplified the transport problem to a within-group, isotropic scattering problem, with constant cross sections within each discrete volume and a steady state external source.

A. Finite Element Equations

We begin by defining finite element notations and apply them to the weak form of the lumped transport equation, and weak form of the lumped transport correction equation (both of which were derived in the first chapter).

1. Transport Finite Element Method

We now derive what we shall call the discrete lumped transport equation. We use a finite element approximation to the spatial dependence of all unknown functions which appear in the transport equation. We choose a separate set of basis functions,

$\underline{b}_\tau(\vec{r})$, to represent the spatial dependence of each unknown function for each cell τ. (We remind that the set is denoted by an underscore, because it is a mathematical column vector.) Each set of basis functions has support only within the cell for which it is defined, and there is a set of bases per cell. We choose a Galerkin weighting; that is, the weight functions are represented by the same bases as the unknown functions. This representation is given by:

$$\begin{aligned} w(\vec{r}) &= \underline{b}_\tau^T(\vec{r}), \underline{W} \\ \psi\left(\vec{r},\vec{\Omega}\right) &= \underline{b}_\tau^T(\vec{r})\,\underline{\psi}\left(\vec{\Omega}\right), \\ \phi(\vec{r}) &= \underline{b}_\tau^T(\vec{r}).\underline{\phi} \end{aligned} \tag{2.1}$$

We substitute these definitions into the weak form of the lumped transport equation, Eq. (1.6):

$$\underline{W}^T \left[\begin{array}{l} \displaystyle\int_{\partial\tau} d^2r\vec{n}(\vec{r})\cdot\vec{\Omega}\underline{b}_\tau(\vec{r})\,\underline{b}_\tau^T(\vec{r})\left[\underline{\psi}_{\partial\tau}^{(l+1/2)}\left(\vec{\Omega}\right)-\underline{\psi}^{(l+1/2)}\left(\vec{\Omega}\right)\right] \\ \displaystyle+\int_\tau d^3r\vec{\Omega}\cdot\underline{b}_\tau(\vec{r})\,\vec{\nabla}\underline{b}_\tau^T(\vec{r})\,\underline{\psi}^{(l+1/2)}\left(\vec{\Omega}\right) \\ \displaystyle+\int_\tau d^3r\sigma_t\underline{b}_\tau(\vec{r})\,\underline{b}_\tau^T(\vec{r})\,\underline{\psi}^{(l+1/2)}\left(\vec{\Omega}\right) \\ \displaystyle=\int_\tau d^3r\frac{\sigma_s}{4\pi}\underline{b}_\tau(\vec{r})\,\underline{b}_\tau^T(\vec{r})\int_{4\pi}d\Omega'\underline{\psi}^{(l)}\left(\vec{\Omega}'\right)+\int_\tau d^3r\underline{b}_\tau(\vec{r})\,Q\left(\vec{r},\vec{\Omega}\right) \end{array} \right]. \tag{2.2}$$

We can see that Eq. (2.2) holds for any vector of weight coefficients, $\underline{W}$, and thus $\underline{W}$ is omitted from further equations. The surface integral is computed by a summation

over each surface of the element:

$$\begin{aligned}&\int_{\partial\tau} d^2r\vec{n}\left(\vec{r}\right)\cdot\vec{\Omega}\underline{b}_\tau\left(\vec{r}\right)\underline{b}_\tau^T\left(\vec{r}\right)\underline{\psi}_{\partial\tau}^{(l+1/2)}\left(\vec{\Omega}\right)\\&=\sum_{k\in\partial\tau}\int_{\partial\tau_k} d^2r\vec{n}_k\left(\vec{r}\right)\cdot\vec{\Omega}\underline{b}_\tau\left(\vec{r}\right)\underline{b}_\tau^T\left(\vec{r}\right)\underline{\psi}_k^{(l+1/2)}\left(\vec{\Omega}\right).\end{aligned}\tag{2.3}$$

At the discontinuity at surface k we choose the upstream quantity:

$$\underline{\psi}_k^{(l+1/2)}\left(\vec{\Omega}\right)=\begin{cases}\underline{\psi}_{k^+}^{(l+1/2)}\left(\vec{\Omega}\right) & \vec{n}_k\left(\vec{r}\right)\cdot\vec{\Omega}<0\\ \underline{\psi}^{(l+1/2)}\left(\vec{\Omega}\right) & \vec{n}_k\left(\vec{r}\right)\cdot\vec{\Omega}>0\end{cases}.\tag{2.4}$$

The subscript k^+ denotes the substitution of upstream unknown from adjacent cell with shared face k. The summation over faces can then be split into incoming and outgoing quantities.

$$\begin{aligned}&\sum_{\partial\tau_k\in\partial\tau}\int_{\partial\tau_k} d^2r\vec{n}_k\left(\vec{r}\right)\cdot\vec{\Omega}\underline{b}_\tau\left(\vec{r}\right)\underline{b}_\tau^T\left(\vec{r}\right)\underline{\psi}_k^{(l+1/2)}\left(\vec{\Omega}\right)\\&=\sum_{\vec{n}_k\cdot\vec{\Omega}<0}\int_{\partial\tau_k} d^2r\vec{n}_k\left(\vec{r}\right)\cdot\vec{\Omega}\underline{b}_\tau\left(\vec{r}\right)\underline{b}_\tau^T\left(\vec{r}\right)\underline{\psi}_{k^+}^{(l+1/2)}\left(\vec{\Omega}\right)\\&+\sum_{\vec{n}_k\cdot\vec{\Omega}>0}\int_{\partial\tau_k} d^2r\vec{n}_k\left(\vec{r}\right)\cdot\vec{\Omega}\underline{b}_\tau\left(\vec{r}\right)\underline{b}_\tau^T\left(\vec{r}\right)\underline{\psi}^{(l+1/2)}\left(\vec{\Omega}\right).\end{aligned}\tag{2.5}$$

The weak form of the lumped transport equation with upstream quantities substituted

on surfaces is:

$$\begin{aligned}
&\sum_{\vec{n}_k\cdot\vec{\Omega}<0}\int_{\partial\tau_k} d^2r\vec{n}_k\left(\vec{r}\right)\cdot\vec{\Omega}\underline{b}_\tau\left(\vec{r}\right)\underline{b}_\tau^T\left(\vec{r}\right)\left[\underline{\psi}_{k^+}^{(l+1/2)}\left(\vec{\Omega}\right)-\underline{\psi}^{(l+1/2)}\left(\vec{\Omega}\right)\right]\\
&+\int_\tau d^3r\vec{\Omega}\cdot\underline{b}_\tau\left(\vec{r}\right)\vec{\nabla}\underline{b}_\tau^T\left(\vec{r}\right)\underline{\psi}^{(l+1/2)}\left(\vec{\Omega}\right)\\
&+\int_\tau d^3r\sigma_t\underline{b}_\tau\left(\vec{r}\right)\underline{b}_\tau^T\left(\vec{r}\right)\underline{\psi}^{(l+1/2)}\left(\vec{\Omega}\right)\\
&=\int_\tau d^3r\frac{\sigma_s}{4\pi}\underline{b}_\tau\left(\vec{r}\right)\underline{b}_\tau^T\left(\vec{r}\right)\int_{4\pi}d\Omega'\underline{\psi}^{(l)}\left(\vec{\Omega}'\right)+\int_\tau d^3r\underline{b}_\tau\left(\vec{r}\right)Q\left(\vec{r},\vec{\Omega}\right).
\end{aligned}\tag{2.6}$$

We now introduce terminology used to represent matrices resulting from the FEM. Matrices are denoted by symbols such as $\underline{\underline{A}}_\Gamma^{pq}$; the superscripts describe the order of the gradient on the basis functions from weight, p, and basis, q, functions respectively; the symbol Γ denotes the domain of the integral, whether it be a surface, $\partial\tau_k$, or volume, τ, integral; the double underscore denotes a matrix. A single underscore denotes a mathematical vector, which may be multiplied by a matrix. We define the following matrices:

$$\begin{aligned}
\underline{\underline{A}}_\tau^{00}&=\int_\tau d^3r\underline{b}_\tau\left(\vec{r}\right)\underline{b}_\tau^T\left(\vec{r}\right),\\
\underline{\underline{\vec{A}}}_\tau^{10}&=\int_\tau d^3r\vec{\nabla}\underline{b}_\tau\left(\vec{r}\right)\underline{b}_\tau^T\left(\vec{r}\right),\\
\underline{\underline{\vec{A}}}_\tau^{01}&=\int_\tau d^3r\underline{b}_\tau\left(\vec{r}\right)\vec{\nabla}\underline{b}_\tau^T\left(\vec{r}\right),\\
\underline{\underline{\vec{A}}}_{\partial\tau_k}^{00}&=\int_{\partial\tau_k} d^2r\vec{n}_k\left(\vec{r}\right)\underline{b}_\tau\left(\vec{r}\right)\underline{b}_\tau^T\left(\vec{r}\right).
\end{aligned}\tag{2.7}$$

Using this notation we obtain the discrete lumped transport equation:

$$\begin{aligned}
&\sum_{\vec{n}_k\cdot\vec{\Omega}<0} \vec{\Omega}\cdot\vec{\underline{\underline{A}}}^{00}_{\partial\tau_k}\left[\underline{\psi}^{(l+1/2)}_{k^+}\left(\vec{\Omega}\right)-\underline{\psi}^{(l+1/2)}\left(\vec{\Omega}\right)\right] \\
&+\vec{\Omega}\cdot\vec{\underline{\underline{A}}}^{01}_{\tau}\,\underline{\psi}^{(l+1/2)}\left(\vec{\Omega}\right) \\
&+\sigma_t\underline{\underline{A}}^{00}_{\tau}\underline{\psi}^{(l+1/2)}\left(\vec{\Omega}\right) \\
&=\frac{\sigma_s}{4\pi}\underline{\underline{A}}^{00}_{\tau}\int_{4\pi}d\Omega'\underline{\psi}^{(l)}\left(\vec{\Omega}'\right)+\int_{\tau}d^3r\underline{b}_{\tau}\left(\vec{r}\right)Q\left(\vec{r},\vec{\Omega}\right).
\end{aligned} \tag{2.8}$$

This equation is the unaccelerated iteration method. Note we have not made any approximations to angle dependence, though it is necessary to make an approximation to angle in order to solve this equation for almost any practical problem.

2. Transport Correction Finite Element Method

We define a discrete correction similar to the functional correction in Eq. (1.7):

$$\underline{f}\left(\vec{\Omega}\right)=\underline{\psi}\left(\vec{\Omega}\right)-\underline{\psi}^{(l+1/2)}\left(\vec{\Omega}\right). \tag{2.9}$$

We subtract the discrete lumped transport equation, Eq. (2.8), from a converged discrete lumped transport equation, and use the discrete correction definition to obtain the discrete lumped transport correction equation:

$$\begin{aligned}
&\sum_{\vec{n}_k\cdot\vec{\Omega}<0}\vec{\Omega}\cdot\vec{\underline{\underline{A}}}^{00}_{\partial\tau_k}\left[\underline{f}_{k^+}\left(\vec{\Omega}\right)-\underline{f}\left(\vec{\Omega}\right)\right]+\vec{\Omega}\cdot\vec{\underline{\underline{A}}}^{01}_{\tau}\,\underline{f}\left(\vec{\Omega}\right) \\
&+\sigma_t\underline{\underline{A}}^{00}_{\tau}\,\underline{f}\left(\vec{\Omega}\right)-\frac{\sigma_s}{4\pi}\underline{\underline{A}}^{00}_{\tau}\int_{4\pi}d\Omega'\,\underline{f}\left(\vec{\Omega}'\right)=\frac{\sigma_s}{4\pi}\underline{\underline{A}}^{00}_{\tau}\left[\underline{\phi}^{(l+1/2)}-\underline{\phi}^{(l)}\right].
\end{aligned} \tag{2.10}$$

We will use this equation to derive lower-order consistent and the proposed methods.

B. Consistent DSA

Early versions of DSA were implemented with limited success and were ineffective for many problems.[5] However, it was well known that the analysis of DSA with no spatial discretization promised spectacular results. It was also observed that different diffusion equation discretization performed differently for identical problems. This led Alcouffe to discover that it was the discretization of the low order equation which must match, or be "consistent" with, the transport discretization.[3] The low order equations performed poorly because they inadvertently made spatial approximations that were not beneficial to acceleration. To ensure spatial consistency, Larsen and co-workers developed a four step procedure to obtain a low order equation for use in a DSA method for virtually any transport spatial discretization, where as Alcouffe's work had applied only to the diamond differencing method.[6] The resulting consistent set of low order equations is important to discuss because it is known to provide effective acceleration and thus serves as a valuable starting point for the creation of methods that may also be effective while being less computationally costly. The consistent low-order equations for DFEM transport as described by the four step procedure are derived as follows.

The first step is to define a correction to the transport variables, Eq. (1.7), and manipulate the iterative transport equation, Eq. (1.3), to obtain the transport correction equation, Eq. (1.8). We then discretize spatially and obtain the discrete transport correction equation, Eq. (2.10). Since this has already been detailed, we continue with the next step.

Step two is to make the P1 angular approximation to the discrete transport correction, and obtain 0th and 1st moments of the discrete correction equation. The P1 approximation to the discrete correction is:

$$\underline{f}\left(\vec{\Omega}\right) = \frac{1}{4\pi}\left[\underline{F} + 3\vec{\Omega}\cdot\underline{\vec{G}}\right]. \tag{2.11}$$

We insert the P1 angular approximation to the discrete transport correction equation:

$$\begin{aligned}
&\sum_{\vec{n}_k\cdot\vec{\Omega}<0} \vec{\Omega}\cdot\underline{\underline{\vec{A}}}^{00}_{\partial\tau_k}\left[\frac{1}{4\pi}\left[\underline{F}_{k^+} + 3\vec{\Omega}\cdot\underline{\vec{G}}_{k^+}\right] - \frac{1}{4\pi}\left[\underline{F} + 3\vec{\Omega}\cdot\underline{\vec{G}}\right]\right] \\
&+ \vec{\Omega}\cdot\underline{\underline{\vec{A}}}^{01}_{\tau}\frac{1}{4\pi}\left[\underline{F} + 3\vec{\Omega}\cdot\underline{\vec{G}}\right] + \sigma_t\underline{\underline{A}}^{00}_{\tau}\frac{1}{4\pi}\left[\underline{F} + 3\vec{\Omega}\cdot\underline{\vec{G}}\right] \\
&- \frac{\sigma_s}{4\pi}\underline{\underline{A}}^{00}_{\tau}\int_{4\pi} d\Omega'\frac{1}{4\pi}\left[\underline{F} + 3\vec{\Omega}'\cdot\underline{\vec{G}}\right] = \frac{\sigma_s}{4\pi}\underline{\underline{A}}^{00}_{\tau}\left[\underline{\phi}^{(l+1/2)} - \underline{\phi}^{(l)}\right].
\end{aligned} \tag{2.12}$$

We take the 0th, $\int_{4\pi} d\Omega$, and 1st, $\int_{4\pi} d\Omega\vec{\Omega}$, angular moments of the P1 discrete transport correction equation, Eq. (2.12):

$$\begin{aligned}
&\int_{4\pi} d\Omega \sum_{\vec{n}_k\cdot\vec{\Omega}<0} \vec{\Omega}\cdot\underline{\underline{\vec{A}}}^{00}_{\partial\tau_k}\left[\frac{1}{4\pi}\left[\underline{F}_{k^+} + 3\vec{\Omega}\cdot\underline{\vec{G}}_{k^+}\right] - \frac{1}{4\pi}\left[\underline{F} + 3\vec{\Omega}\cdot\underline{\vec{G}}\right]\right] \\
&+ \underline{\underline{\vec{A}}}^{01}_{\tau}\cdot\underline{\vec{G}} + \sigma_a\underline{\underline{A}}^{00}_{\tau}\underline{F} = \sigma_s\underline{\underline{A}}^{00}_{\tau}\left[\underline{\phi}^{(l+1/2)} - \underline{\phi}^{(l)}\right],
\end{aligned} \tag{2.13}$$

$$\begin{aligned}
&\sum_{\vec{n}_k\cdot\vec{\Omega}<0} \int_{4\pi} d\Omega\vec{\Omega}\vec{\Omega}\cdot\underline{\underline{\vec{A}}}^{00}_{\partial\tau_k}\left[\frac{1}{4\pi}\left[\underline{F}_{k^+} + 3\vec{\Omega}\cdot\underline{\vec{G}}_{k^+}\right] - \frac{1}{4\pi}\left[\underline{F} + 3\vec{\Omega}\cdot\underline{\vec{G}}\right]\right] \\
&+ \underline{\underline{\vec{A}}}^{01}_{\tau}\frac{1}{3}\underline{F} + \sigma_t\underline{\underline{A}}^{00}_{\tau}\underline{\vec{G}} = 0,
\end{aligned} \tag{2.14}$$

where:

$$\sigma_a = \sigma_t - \sigma_s. \tag{2.15}$$

The integrals that have not been evaluated are surface integrals. How they are handled depends on geometry, angular discretization, and approximations (e.g. upwind, downwind, etc.). The surface terms couple the entire problem spatially. The scalar and vector equations are coupled to each other as well. In three dimensions, this is a system of four equations for four sets of unknowns. In the special case of Cartesian geometry and values taken from upstream, the 0th and 1st moment equations become:

$$\begin{aligned}&\sum_{\partial\tau_k\in\partial\tau} \vec{\underline{\underline{A}}}^{00}_{\partial\tau_k} \cdot \left[-\vec{\alpha}_{k,1}\left(\underline{F}_{k^+} - \underline{F}\right) + 3\alpha_2\left(\vec{\underline{G}}_{k^+} - \vec{\underline{G}}\right)\right] \\ &+ \vec{\underline{\underline{A}}}^{01}_{\tau} \cdot \vec{\underline{G}} + \sigma_a \underline{\underline{A}}^{00}_{\tau}\,\underline{F} = \sigma_s \underline{\underline{A}}^{00}_{\tau}\left[\underline{\phi}^{(l+1/2)} - \underline{\phi}^{(l)}\right],\end{aligned} \tag{2.16}$$

$$\begin{aligned}&\sum_{\partial\tau_k\in\partial\tau} \left[\alpha_2 \vec{\underline{\underline{A}}}^{00}_{\partial\tau_k}\left(\underline{F}_{k^+} - \underline{F}\right) - 3\vec{\underline{\underline{A}}}^{00}_{\partial\tau_k} \cdot \vec{\vec{\alpha}}_{k,3} \cdot \left(\vec{\underline{G}}_{k^+} - \vec{\underline{G}}\right)\right] \\ &+ \vec{\underline{\underline{A}}}^{01}_{\tau}\frac{1}{3}\underline{F} + \sigma_t \underline{\underline{A}}^{00}_{\tau}\vec{\underline{G}} = 0,\end{aligned} \tag{2.17}$$

where,

$$\begin{aligned}
\vec{\alpha}_{k,1} &= \frac{1}{4\pi}\int_{\vec{n}_k\cdot\vec{\Omega}>0} d\Omega\vec{\Omega} = -\frac{1}{4\pi}\int_{\vec{n}_k\cdot\vec{\Omega}<0} d\Omega\vec{\Omega}, \\
\vec{\vec{\alpha}}_{k,2} &= \frac{1}{4\pi}\int_{\vec{n}_k\cdot\vec{\Omega}>0} d\Omega\vec{\Omega}\vec{\Omega} = \frac{1}{4\pi}\int_{\vec{n}_k\cdot\vec{\Omega}<0} d\Omega\vec{\Omega}\vec{\Omega} = \alpha_2\vec{\vec{I}}, \\
\vec{\vec{\vec{\alpha}}}_{k,3} &= \frac{1}{4\pi}\int_{\vec{n}_k\cdot\vec{\Omega}>0} d\Omega\vec{\Omega}\vec{\Omega}\vec{\Omega} = -\frac{1}{4\pi}\int_{\vec{n}_k\cdot\vec{\Omega}<0} d\Omega\vec{\Omega}\vec{\Omega}\vec{\Omega}.
\end{aligned} \tag{2.18}$$

As single arrow denotes a vector, multiple arrows denote higher rank tensors obtained from tensor products of the direction vectors.

Step three is to solve the coupled systems of equations for $\underline{F}$ and $\vec{\underline{G}}$ simultaneously.

Step four is to update the transport scalar quantity with the usual update equation:

$$\underline{\phi}^{(l+1)} = \underline{\phi}^{(l+1/2)} + \underline{F}. \tag{2.19}$$

When this method has been applied to most discrete transport equations it has yielded the behavior expected from the non discrete DSA analysis.[1] However, there are several considerable drawbacks that have made this method inconvenient or inefficient. It has been found that this method may be poorly conditioned due to relative sizes of scalar and vector variables. It has also been found that this method is costly to solve.[7] Multiple systems of equations coupled throughout the problem domain drastically increases the size of the linear system of equations. For many practical problems, this method takes more computational time than is gained from acceleration of the original problem.

The transport DFEM introduces coupling to adjacent cells through surface quantities. For the low-order equation to have the same representation of importance of unknowns, the effects of this surface coupling must be included. When comparing the continuous diffusion correction equation to the system of discontinuous correction equations, the coupling and matrices are markedly different. The continuous equations do not allow for coupling through surface terms, as the surface is equal from both sides of a face. The naive treatment of discretization (performing linear operations to eliminate quantities prior to discretization) results in different surface and "stiffness" matrices, as we will see in the next section.

C. Inconsistent DSA

The simplest of the methods discussed in this thesis, an inconsistent DSA method, results from the P_1 approximation to the non-discrete transport correction equation. We then use a continuous finite element method (CFEM) for our low-angular-order corrections, and apply the continuous corrections to the discontinuous transport iteration without any modifications. This cavalier treatment of discretization results in a low order equation which is incompatible with the transport equation in many important limits.

1. P_1 Approximation to Transport Correction Equation

We begin with the transport correction in Eq. (1.8). We approximate the transport correction $f\left(\vec{r},\vec{\Omega}\right)$ with a P_1 approximation to the angular distribution:

$$f\left(\vec{r},\vec{\Omega}\right)\approx\frac{1}{4\pi}\left[F\left(\vec{r}\right)+3\vec{\Omega}\cdot\vec{G}\left(\vec{r}\right)\right]. \tag{2.20}$$

Here $F\left(\vec{r}\right)$ is a 0^{th} order (scalar) correction, and $\vec{G}\left(\vec{r}\right)$ is a vector of 1^{st} order (current) corrections. Applying the P_1 approximation to the transport correction equation:

$$\begin{aligned}&\vec{\Omega}\cdot\vec{\nabla}\frac{1}{4\pi}\left[F\left(\vec{r}\right)+3\vec{\Omega}\cdot\vec{G}\left(\vec{r}\right)\right]+\sigma_t\frac{1}{4\pi}\left[F\left(\vec{r}\right)+3\vec{\Omega}\cdot\vec{G}\left(\vec{r}\right)\right]\\&-\frac{\sigma_s}{4\pi}\int_{4\pi}d\Omega'\frac{1}{4\pi}\left[F\left(\vec{r}\right)+3\vec{\Omega}'\cdot\vec{G}\left(\vec{r}\right)\right]\\&=\frac{\sigma_s}{4\pi}\left[\phi^{(l+1/2)}\left(\vec{r}\right)-\phi^{(l)}\left(\vec{r}\right)\right].\end{aligned} \tag{2.21}$$

Taking the 0^{th} and 1^{st} angular moments by operating on Eq. (2.21) by $\int_{4\pi}d\Omega$ and $\int_{4\pi}d\Omega\vec{\Omega}$ respectively:

$$\vec{\nabla}\cdot\vec{G}\left(\vec{r}\right)+\left(\sigma_t-\sigma_s\right)F\left(\vec{r}\right)=\sigma_s\left[\phi^{(l+1/2)}\left(\vec{r}\right)-\phi^{(l)}\left(\vec{r}\right)\right], \tag{2.22}$$

$$\frac{1}{3}\vec{\nabla}F\left(\vec{r}\right)+\sigma_t\vec{G}\left(\vec{r}\right)=0. \tag{2.23}$$

We eliminate the 1^{st} order correction from Eq. (2.22), with no discretion toward

discretization, to obtain a diffusion equation for the 0^{th} order correction:

$$-\vec{\nabla}\cdot\frac{1}{3\sigma_t}\vec{\nabla}F\left(\vec{r}\right)+\sigma_a F\left(\vec{r}\right)=\sigma_s\left[\phi^{(l+1/2)}\left(\vec{r}\right)-\phi^{(l)}\left(\vec{r}\right)\right]. \tag{2.24}$$

2. Continuous FEM Diffusion Correction Equation

To the diffusion correction equation, we apply a continuous FEM with basis functions for each support equal to the corresponding discontinuous basis function in the mesh of interest. We choose a continuous FEM for the lower number of unknowns, and to compare to our proposed method. In a later section, we use this same system of equations for one of two main steps for obtaining the corrections for the proposed method.

We begin by taking a weighted integral of the diffusion correction equation, Eq. (2.24), over the problem domain:

$$\int_\Gamma d^3r w\left(\vec{r}\right)\left(-\vec{\nabla}\cdot\frac{1}{3\sigma_t}\vec{\nabla}F\left(\vec{r}\right)+\sigma_a F\left(\vec{r}\right)=\sigma_s\left[\phi^{(l+1/2)}\left(\vec{r}\right)-\phi^{(l)}\left(\vec{r}\right)\right]\right). \tag{2.25}$$

We use the divergence theorem to obtain a weak form of the equation, since the second derivative of the basis function often does not exist:

$$\begin{aligned}&-\int_{\partial\Gamma}d^2rn\left(\vec{r}\right)w\left(\vec{r}\right)\cdot\frac{1}{3\sigma_t}\vec{\nabla}F\left(\vec{r}\right)+\int_\Gamma d^3r\vec{\nabla}w\left(\vec{r}\right)\cdot\frac{1}{3\sigma_t}\vec{\nabla}F\left(\vec{r}\right)\\&+\int_\Gamma d^3rw\left(\vec{r}\right)\sigma_a F\left(\vec{r}\right)=\int_\Gamma d^3rw\left(\vec{r}\right)\sigma_s\left[\phi^{(l+1/2)}\left(\vec{r}\right)-\phi^{(l)}\left(\vec{r}\right)\right].\end{aligned} \tag{2.26}$$

We expand correction variables in a continuous basis with supports at each node and add a subscript, C, to correction variables to denote Continuous corrections:

$$F\left(\vec{r}\right) = \underline{b}_{\tau}^{T}\left(\vec{r}\right)\underline{\underline{H}}_{\tau}\underline{F}_{C}. \tag{2.27}$$

Here $\underline{\underline{H}}_{\tau}$ maps the continuous basis into the discontinuous basis of element τ, and $\underline{F}_{C}$ is the vector of continuous corrections with corresponding supports in element τ. The operation of $\underline{\underline{H}}_{\tau}$ is simple: it selects from the continuous correction array the unknown associated with the associated element, and places it in the corresponding row. We expand the scalar variable in a discontinuous basis, which is non-zero only within the element it is designated to. We define a vector of weight functions for mesh τ expanded in a continuous basis in a similar manner:

$$w_{\tau}\left(\vec{r}\right) = \underline{W}_{C}^{T}\underline{\underline{H}}_{\tau}^{T}\underline{b}_{\tau}\left(\vec{r}\right). \tag{2.28}$$

The purpose of $\underline{\underline{H}}_{\tau}^{T}$ in the weight function expansion is to select which rows of the system are influenced by element τ. For the continuous FEM, each basis function is non-zero in all neighboring elements. Thus we cannot convert the integral into an equation for one element; instead we must take a summation of all elements of the mesh to obtain a system of equations, which couples all unknowns in the continuous

system. We omit the weight coefficient vector for simplicity:

$$\begin{aligned}
&-\sum_{\partial\tau\in\partial\Gamma}\underline{\underline{H}}_{\tau}^{T}\frac{1}{3\sigma_t}\int_{\partial\tau}d^2r\vec{n}\left(\vec{r}\right)\cdot\underline{b}_{\tau}\left(\vec{r}\right)\vec{\nabla}\underline{b}_{\tau}^{T}\left(\vec{r}\right)\underline{\underline{H}}_{\tau}\underline{F}_{C}\\
&+\sum_{\tau\in\Gamma}\underline{\underline{H}}_{\tau}^{T}\frac{1}{3\sigma_t}\int_{\tau}d^3r\vec{\nabla}\underline{b}_{\tau}\left(\vec{r}\right)\cdot\vec{\nabla}\underline{b}_{\tau}^{T}\left(\vec{r}\right)\underline{\underline{H}}_{\tau}\underline{F}_{C}\\
&+\sum_{\tau\in\Gamma}\underline{\underline{H}}_{\tau}^{T}\sigma_a\int_{\tau}d^3r\underline{b}_{\tau}\left(\vec{r}\right)\underline{b}_{\tau}^{T}\left(\vec{r}\right)\underline{\underline{H}}_{\tau}\underline{F}_{C}\\
&=\sum_{\tau\in\Gamma}\underline{\underline{H}}_{\tau}^{T}\sigma_s\int_{\tau}d^3r\underline{b}_{\tau}\left(\vec{r}\right)\underline{b}_{\tau}^{T}\left(\vec{r}\right)\left(\underline{\phi}^{(l+1/2)}-\underline{\phi}^{(l)}\right).
\end{aligned}\tag{2.29}$$

We define two diffusion matrices to succinctly write the continuous diffusion correction equation:

$$\begin{aligned}
\underline{\underline{\vec{A}}}_{\partial\tau}^{01}&=\int_{\partial\tau\in\partial\Gamma}d^2r\underline{b}_{\tau}\left(\vec{r}\right)\vec{\nabla}\underline{b}_{\tau}^{T}\left(\vec{r}\right),\\
\underline{\underline{A}}_{\tau}^{11}&=\int_{\tau\in\Gamma}d^3r\vec{\nabla}\underline{b}_{\tau}\left(\vec{r}\right)\cdot\vec{\nabla}\underline{b}_{\tau}^{T}\left(\vec{r}\right).
\end{aligned}\tag{2.30}$$

The continuous diffusion correction equation is given by the following:

$$\begin{aligned}
&-\sum_{\partial\tau\in\partial\Gamma}\underline{\underline{H}}_{\tau}^{T}\frac{1}{3\sigma_t}\vec{n}_{\partial\tau}\cdot\underline{\underline{\vec{A}}}_{\partial\tau}^{01}\underline{\underline{H}}_{\tau}\underline{F}_{C}\\
&+\sum_{\tau\in\Gamma}\underline{\underline{H}}_{\tau}^{T}\frac{1}{3\sigma_t}\underline{\underline{A}}_{\tau}^{11}\underline{\underline{H}}_{\tau}\underline{F}_{C}\\
&+\sum_{\tau\in\Gamma}\underline{\underline{H}}_{\tau}^{T}\sigma_a\underline{\underline{A}}_{\tau}^{00}\underline{\underline{H}}_{\tau}\underline{F}_{C}\\
&=\sum_{\tau\in\Gamma}\underline{\underline{H}}_{\tau}^{T}\sigma_s\underline{\underline{A}}_{\tau}^{00}\left(\underline{\phi}^{(l+1/2)}-\underline{\phi}^{(l)}\right).
\end{aligned}\tag{2.31}$$

After solving the previous system of equations for $\underline{F}_C$, we naively use this value to

correct our scalar variable in each element:

$$\underline{\phi}^{(l+1)} = \underline{\phi}^{(l+1/2)} + \underline{\underline{H}}_{\tau}\underline{F}_{C}. \tag{2.32}$$

At first glance, this method has promise. It uses a good approximation to the original problem to accelerate convergence. Indeed we will later find that in some cases, such as thin square cells with isotropic scattering, convergence is accelerated. In more strenuous cases, such as problems with optically thick cells, ironically where theory would suggest a diffusion approximation should be valid, the method degrades. Figures containing the exact behavior of this method may be found in the Method Analysis chapter.

3. Approximation to Stiffness Matrix

When implementing an acceleration method to an existing code, it is valuable for the method to not require reevaluation of finite element bases to obtain new matrices, or storage for these matrices. We manipulate the P_1 diffusion equations to obtain a continuous finite element diffusion method that does not require additional matrices or storage. The result is an approximation to the stiffness matrix in terms of matrices already defined in transport calculations. In the analysis section we show the approximate matrix does not cause significant degradation of spectral radius of the operator. We begin with the 0th and 1st moments of the P_1 approximation to transport correction equation:

$$\vec{\nabla} \cdot \vec{G}\left(\vec{r}\right) + \left(\sigma_t - \sigma_s\right) F\left(\vec{r}\right) = \sigma_s \left[\phi^{(l+1/2)}\left(\vec{r}\right) - \phi^{(l)}\left(\vec{r}\right)\right], \tag{2.33}$$

$$\frac{1}{3}\vec{\nabla}F\left(\vec{r}\right)+\sigma_t\vec{G}\left(\vec{r}\right)=0. \tag{2.34}$$

This time, we apply a continuous FEM to the equations before eliminating $\vec{G}$ from the equations:

$$\begin{aligned}
&\sum_{\tau\in\Gamma}\underline{\underline{H}}_{\tau}^{T}\int_{\tau}d^{3}r\underline{b}_{\tau}\left(\vec{r}\right)\vec{\nabla}\underline{b}_{\tau}^{T}\left(\vec{r}\right)\underline{\underline{H}}_{\tau}\cdot\underline{\vec{G}}_{C}\\
&+\sum_{\tau\in\Gamma}\left(\sigma_t-\sigma_s\right)\underline{\underline{H}}_{\tau}^{T}\int_{\tau}d^{3}r\underline{b}_{\tau}\left(\vec{r}\right)\underline{b}_{\tau}^{T}\left(\vec{r}\right)\underline{\underline{H}}_{\tau}\underline{F}_{C}\\
&=\sum_{\tau\in\Gamma}\underline{\underline{H}}_{\tau}^{T}\sigma_s\int_{\tau}d^{3}r\underline{b}_{\tau}\left(\vec{r}\right)\underline{b}_{\tau}^{T}\left(\vec{r}\right)\left(\underline{\phi}^{(l+1/2)}-\underline{\phi}^{(l)}\right),
\end{aligned} \tag{2.35}$$

$$\frac{1}{3}\sum_{\tau\in\Gamma}\underline{\underline{H}}_{\tau}^{T}\int_{\tau}d^{3}r\underline{b}_{\tau}\left(\vec{r}\right)\vec{\nabla}\underline{b}_{\tau}^{T}\left(\vec{r}\right)\underline{\underline{H}}_{\tau}\underline{F}_{C}+\sum_{\tau\in\Gamma}\sigma_t\underline{\underline{H}}_{\tau}^{T}\int_{\tau}d^{3}r\underline{b}_{\tau}\left(\vec{r}\right)\underline{b}_{\tau}^{T}\left(\vec{r}\right)\underline{\underline{H}}_{\tau}\cdot\underline{\vec{G}}_{C}=0. \tag{2.36}$$

We use the divergence theorem on the gradient in the 0th moment equation to obtain quantities on the boundary of the domain:

$$\begin{aligned}
&\sum_{\partial\tau\in\partial\Gamma}\underline{\underline{H}}_{\tau}^{T}\int_{\partial\tau}d^{2}r\vec{n}\left(\vec{r}\right)\underline{b}_{\tau}\left(\vec{r}\right)\underline{b}_{\tau}^{T}\left(\vec{r}\right)\underline{\underline{H}}_{\tau}\cdot\underline{\vec{G}}_{C}\\
&-\sum_{\tau\in\Gamma}\underline{\underline{H}}_{\tau}^{T}\int_{\tau}d^{3}r\vec{\nabla}\underline{b}_{\tau}\left(\vec{r}\right)\underline{b}_{\tau}^{T}\left(\vec{r}\right)\underline{\underline{H}}_{\tau}\cdot\underline{\vec{G}}_{C}\\
&+\sum_{\tau\in\Gamma}\left(\sigma_t-\sigma_s\right)\underline{\underline{H}}_{\tau}^{T}\int_{\tau}d^{3}r\underline{b}_{\tau}\left(\vec{r}\right)\underline{b}_{\tau}^{T}\left(\vec{r}\right)\underline{\underline{H}}_{\tau}\underline{F}_{C}\\
&=\sum_{\tau\in\Gamma}\underline{\underline{H}}_{\tau}^{T}\sigma_s\int_{\tau}d^{3}r\underline{b}_{\tau}\left(\vec{r}\right)\underline{b}_{\tau}^{T}\left(\vec{r}\right)\left(\underline{\phi}^{(l+1/2)}-\underline{\phi}^{(l)}\right).
\end{aligned} \tag{2.37}$$

We substitute matrices defined for the transport FEM into the 0th and 1st moment equations:

$$\begin{aligned}&\sum_{\partial\tau\in\partial\Gamma}\underline{\underline{H}}_{\tau}^{T}\vec{\underline{\underline{A}}}_{\partial\tau}^{00}\underline{\underline{H}}_{\tau}\cdot\vec{\underline{G}}_{C}-\sum_{\tau\in\Gamma}\underline{\underline{H}}_{\tau}^{T}\vec{\underline{\underline{A}}}_{\tau}^{10}\underline{\underline{H}}_{\tau}\cdot\vec{\underline{G}}_{C}\\&+\sum_{\tau\in\Gamma}\left(\sigma_{t}-\sigma_{s}\right)\underline{\underline{H}}_{\tau}^{T}\underline{\underline{A}}_{\tau}^{00}\underline{\underline{H}}_{\tau}\underline{F}_{C}=\sum_{\tau\in\Gamma}\underline{\underline{H}}_{\tau}^{T}\sigma_{s}\underline{\underline{H}}_{\tau}^{T}\underline{\underline{A}}_{\tau}^{00}\left(\underline{\phi}^{(l+1/2)}-\underline{\phi}^{(l)}\right),\end{aligned}\tag{2.38}$$

$$\frac{1}{3}\sum_{\tau\in\Gamma}\underline{\underline{H}}_{\tau}^{T}\vec{\underline{\underline{A}}}_{\tau}^{01}\underline{\underline{H}}_{\tau}\underline{F}_{C}+\sum_{\tau\in\Gamma}\sigma_{t}\underline{\underline{H}}_{\tau}^{T}\underline{\underline{A}}_{\tau}^{00}\underline{\underline{H}}_{\tau}\vec{\underline{G}}_{C}=0.\tag{2.39}$$

To eliminate $\vec{\underline{G}}_{C}$ would require solving the system of globally coupled equations. Instead, we pretend we can solve the 1st moment equation uncoupled. We would obtain the same result had we not applied the continuous FEM before solving for $\vec{G}_{C}\left(\vec{r}\right)$. This gives us:

$$\underline{\underline{H}}_{\tau}\vec{\underline{G}}_{C}=-\frac{1}{3\sigma_{t}}\left[\underline{\underline{A}}_{\tau}^{00}\right]^{-1}\vec{\underline{\underline{A}}}_{\tau}^{01}\underline{\underline{H}}_{\tau}\underline{F}_{C}.\tag{2.40}$$

We substitute this expression for $\vec{\underline{G}}_{C}$ into the 0th moment equation; we do not substitute for the boundary quantity, as that is defined by boundary conditions depending on the problem:

$$\begin{aligned}&\sum_{\partial\tau\in\partial\Gamma}\underline{\underline{H}}_{\tau}^{T}\vec{\underline{\underline{A}}}_{\partial\tau}^{00}\underline{\underline{H}}_{\tau}\cdot\vec{\underline{G}}_{C}+\sum_{\tau\in\Gamma}\underline{\underline{H}}_{\tau}^{T}\vec{\underline{\underline{A}}}_{\tau}^{10}\cdot\frac{1}{3\sigma_{t}}\left[\underline{\underline{A}}_{\tau}^{00}\right]^{-1}\vec{\underline{\underline{A}}}_{\tau}^{01}\underline{\underline{H}}_{\tau}\underline{F}_{C}\\&+\sum_{\tau\in\Gamma}\left(\sigma_{t}-\sigma_{s}\right)\underline{\underline{H}}_{\tau}^{T}\underline{\underline{A}}_{\tau}^{00}\underline{\underline{H}}_{\tau}\underline{F}_{C}=\sum_{\tau\in\Gamma}\underline{\underline{H}}_{\tau}^{T}\sigma_{s}\underline{\underline{H}}_{\tau}^{T}\underline{\underline{A}}_{\tau}^{00}\left(\underline{\phi}^{(l+1/2)}-\underline{\phi}^{(l)}\right).\end{aligned}\tag{2.41}$$

This is almost identical to the equation obtained before, except instead of a stiffness matrix we have an expression in terms of transport FEM matrices:

$$\underline{\underline{A}}_{\tau}^{11} \approx \vec{\underline{\underline{A}}}_{\tau}^{10} \cdot \left[\underline{\underline{A}}_{\tau}^{00}\right]^{-1} \vec{\underline{\underline{A}}}_{\tau}^{01} \tag{2.42}$$

D. Proposed DSA

This method follows Wareing's work, which sought which sought to make an inexpensive inconsistent DSA method much closer to the consistent method without adding significant computational cost.[4] Wareing's work was done specifically for linear discontinuous (LD) and bilinear discontinuous (BLD) finite elements in 1D and 2D. As such, the assumptions made have not been generalized to handle various meshes, geometries, and basis functions. We extend that work to arbitrary FEM and arbitrary spatial grids in arbitrary dimension.

The core of Wareing's method is to modify a consistent low order correction by utilizing a simpler inconsistent correction. The resulting method should be sufficiently consistent that it maintains properties of the fully consistent method in practical regimes to the extent possible. In Wareing's method, both the consistent and inconsistent correction equations are obtained via asymptotic scaling of the transport equation. We make the modification of forgoing any attempt at consistency of the inconsistent correction equation, for simplicity's sake. This has the added benefit of demonstrating the flexibility of this method. We will later use an inconsistent method which utilizes only transport matrices.

Specifically, Wareing's method began with a discontinuous transport sweep. He then

solved a continuous-FEM diffusion equation, which was derived from an asymptotic scaling of the discretized continuous FEM transport equation. Lastly, he used the continuous diffusion correction solution to generate a collection of one-cell consistent, discontinuous correction equations, which were derived from a P1 approximation (similar to Larsen's four-step procedure) of the discretized discontinuous FEM transport equation.

We begin our derivation with three sets of equations that have already been defined: the discrete transport equation in Eq. (2.8), the discrete continuous correction equation, Eq. (2.31) from the inconsistent DSA section, and the set of discrete discontinuous correction equations, Eq. (2.13)-(2.14) from the consistent DSA section. We reiterate these equations with one important addition: the continuous correction variables have the subscript C appended to them to denote Continuous, and the discontinuous correction variables have the subscript D, for Discontinuous.

$$\begin{aligned}
&\sum_{\vec{n}_k\cdot\vec{\Omega}<0} \vec{\Omega}\cdot\underline{\underline{\vec{A}}}^{00}_{\partial\tau_k}\left[\underline{\psi}^{(l+1/2)}_{k^+}\left(\vec{\Omega}\right)-\underline{\psi}^{(l+1/2)}\left(\vec{\Omega}\right)\right] \\
&+\vec{\Omega}\cdot\underline{\underline{\vec{A}}}^{01}_{\tau}\,\underline{\psi}^{(l+1/2)}\left(\vec{\Omega}\right) \\
&+\sigma_t\underline{\underline{A}}^{00}_{\tau}\,\underline{\psi}^{(l+1/2)}\left(\vec{\Omega}\right) \\
&=\frac{\sigma_s}{4\pi}\underline{\underline{A}}^{00}_{\tau}\int_{4\pi}d\Omega'\,\underline{\psi}^{(l)}\left(\vec{\Omega}'\right)+\int_{\tau}d^3r\,\underline{b}_{\tau}\left(\vec{r}\right)Q\left(\vec{r},\vec{\Omega}\right),
\end{aligned} \tag{2.43}$$

$$
\begin{aligned}
&- \sum_{\partial\tau\in\partial\Gamma} \underline{\underline{H}}_{\tau}^{T} \frac{1}{3\sigma_t} \vec{n}_{\partial\tau} \cdot \vec{\underline{\underline{A}}}_{\partial\tau}^{01} \underline{\underline{H}}_{\tau} \underline{F}_C \\
&+ \sum_{\tau\in\Gamma} \underline{\underline{H}}_{\tau}^{T} \frac{1}{3\sigma_t} \underline{\underline{A}}_{\tau}^{11} \underline{\underline{H}}_{\tau} \underline{F}_C \\
&+ \sum_{\tau\in\Gamma} \underline{\underline{H}}_{\tau}^{T} \sigma_a \underline{\underline{A}}_{\tau}^{00} \underline{\underline{H}}_{\tau} \underline{F}_C \\
&= \sum_{\tau\in\Gamma} \underline{\underline{H}}_{\tau}^{T} \sigma_s \underline{\underline{A}}_{\tau}^{00} \left(\underline{\phi}^{(l+1/2)} - \underline{\phi}^{(l)} \right),
\end{aligned}
\tag{2.44}
$$

$$
\begin{aligned}
&\sum_{\partial\tau_k\in\partial\tau} \vec{\underline{\underline{A}}}_{\partial\tau_k}^{00} \cdot \left[-\vec{\alpha}_{k,1} \left(\underline{F}_{D,k^+} - \underline{F}_D \right) + 3\alpha_2 \left(\vec{\underline{G}}_{D,k^+} - \vec{\underline{G}}_D \right) \right] \\
&+ \vec{\underline{\underline{A}}}_{\tau}^{01} \cdot \vec{\underline{G}}_D + \sigma_a \underline{\underline{A}}_{\tau}^{00} \underline{F}_D = \sigma_s \underline{\underline{A}}_{\tau}^{00} \left[\underline{\phi}^{(l+1/2)} - \underline{\phi}^{(l)} \right],
\end{aligned}
\tag{2.45}
$$

$$
\begin{aligned}
&\sum_{\partial\tau_k\in\partial\tau} \left[\alpha_2 \vec{\underline{\underline{A}}}_{\partial\tau_k}^{00} \left(\underline{F}_{D,k^+} - \underline{F}_D \right) - 3 \vec{\underline{\underline{A}}}_{\partial\tau_k}^{00} \cdot \vec{\vec{\alpha}}_{k,3} \cdot \left(\vec{\underline{G}}_{D,k^+} - \vec{\underline{G}}_D \right) \right] \\
&+ \vec{\underline{\underline{A}}}_{\tau}^{01} \frac{1}{3} \underline{F}_D + \sigma_t \underline{\underline{A}}_{\tau}^{00} \vec{\underline{G}}_D = 0.
\end{aligned}
\tag{2.46}
$$

Our first step is to approximate the source of coupling in the consistent correction equations, the discontinuities of surface quantities.

$$
\left(\underline{F}_{D,k^+} - \underline{F}_D \right) \approx 2 \left(\underline{\underline{H}}_{\tau} \underline{F}_C - \underline{F}_D \right), \ or \ \frac{1}{2} \left(\underline{F}_{D,k^+} + \underline{F}_D \right) \approx \underline{\underline{H}}_{\tau} \underline{F}_C \tag{2.47}
$$

$$
\left(\vec{\underline{G}}_{D,k^+} - \vec{\underline{G}}_D \right) \approx 0, \ or \ \vec{\underline{G}}_{D,k^+} \approx \vec{\underline{G}}_D. \tag{2.48}
$$

The first approximation is similar to a first order approximation, linearly extrapo-

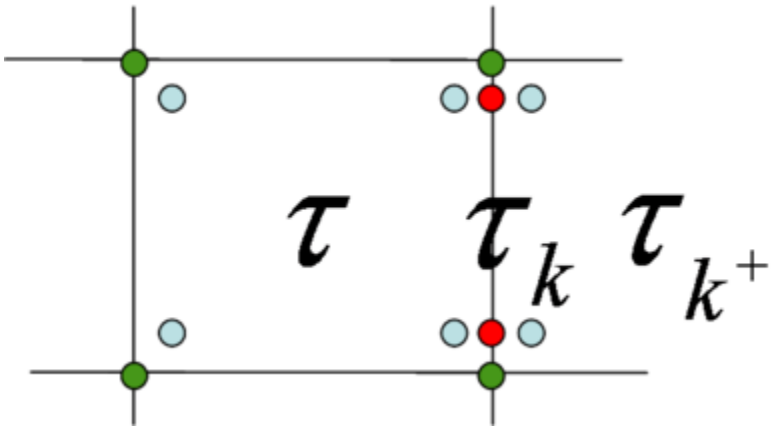

Fig. 1. Continuous (green), discontinuous (blue), and surface (red) quantities.

lating the difference to determine the quantity outside of the element. In Fig. 1 we can see this extrapolation in that the difference between two discontinuous quantities (blue) is twice the difference of the discontinuous quantity in the element and the continuous quantity (green). The second approximation is made due to lack of higher angular moments obtained from the inconsistent equations. If the discontinuity in $\underline{\vec{G}}_D$ is important, then the approximation may be inaccurate and the method may lose effectiveness.

We then insert these approximations into the set of discontinuous correction equations and simplify the results. The resulting set of equations becomes:

$$\begin{aligned}&\sum_{\partial\tau_k\in\partial\tau} \underline{\underline{\vec{A}}}^{00}_{\partial\tau_k} \cdot \left[-\vec{\alpha}_{k,1} 2 \left(\underline{\underline{H}}_\tau \underline{F}_C - \underline{F}_D\right)\right] + \underline{\underline{\vec{A}}}^{01}_{\tau} \cdot \underline{\vec{G}}_D \\ &+ \sigma_a \underline{\underline{A}}^{00}_{\tau} \underline{F}_D = \sigma_s \underline{\underline{A}}^{00}_{\tau} \left(\underline{\phi}^{(l+1/2)} - \underline{\phi}^{(l)}\right),\end{aligned} \tag{2.49}$$

$$\sum_{\partial\tau_k\in\partial\tau} \alpha_2 \underline{\underline{\vec{A}}}^{00}_{\partial\tau_k} 2 \left(\underline{\underline{H}}_\tau \underline{F}_C - \underline{F}_D\right) + \underline{\underline{\vec{A}}}^{01}_{\tau} \frac{1}{3} \underline{F}_D + \sigma_t \underline{\underline{A}}^{00}_{\tau} \underline{\vec{G}}_D = 0. \tag{2.50}$$

We use linear algebra to solve this single element system of equations for $\underline{F}_D$ explicitly.

We solve the 1st moment equation for $\underline{\vec{G}}_D$:

$$\underline{\vec{G}}_D = -\frac{1}{\sigma_t}\left[\underline{\underline{A}}^{00}_{\tau}\right]^{-1}\sum_{\partial\tau_k\in\partial\tau}\alpha_2\underline{\underline{\vec{A}}}^{00}_{\partial\tau_k}2\left(\underline{\underline{H}}_{\tau}\underline{F}_C-\underline{F}_D\right)-\frac{1}{\sigma_t}\left[\underline{\underline{A}}^{00}_{\tau}\right]^{-1}\underline{\underline{\vec{A}}}^{01}_{\tau}\frac{1}{3}\underline{F}_D. \tag{2.51}$$

We substitute the result for $\underline{\vec{G}}_D$ into the 0th moment equation:

$$\begin{aligned}
&\sum_{\partial\tau_k\in\partial\tau}\underline{\underline{\vec{A}}}^{00}_{\partial\tau_k}\cdot\left[-\vec{\alpha}_{k,1}2\left(\underline{\underline{H}}_{\tau}\underline{F}_C-\underline{F}_D\right)\right]\\
&+\underline{\underline{\vec{A}}}^{01}_{\tau}\cdot\left(-\frac{1}{\sigma_t}\left[\underline{\underline{A}}^{00}_{\tau}\right]^{-1}\sum_{\partial\tau_k\in\partial\tau}\alpha_2\underline{\underline{\vec{A}}}^{00}_{\partial\tau_k}2\left(\underline{\underline{H}}_{\tau}\underline{F}_C-\underline{F}_D\right)-\frac{1}{\sigma_t}\left[\underline{\underline{A}}^{00}_{\tau}\right]^{-1}\underline{\underline{\vec{A}}}^{01}_{\tau}\frac{1}{3}\underline{F}_D\right)\\
&+\sigma_a\underline{\underline{A}}^{00}_{\tau}\underline{F}_D=\sigma_s\underline{\underline{A}}^{00}_{\tau}\left(\underline{\phi}^{(l+1/2)}-\underline{\phi}^{(l)}\right),
\end{aligned} \tag{2.52}$$

Finally, we gather like quantities:

$$\begin{aligned}
&\sum_{\partial\tau_k\in\partial\tau}\underline{\underline{\vec{A}}}^{00}_{\partial\tau_k}\cdot\left(-\vec{\alpha}_{k,1}\right)2\underline{\underline{H}}_{\tau}\underline{F}_C\\
&+\sum_{\partial\tau_k\in\partial\tau}\underline{\underline{\vec{A}}}^{00}_{\partial\tau_k}\cdot\left(-\vec{\alpha}_{k,1}\right)2\left(-\underline{F}_D\right)\\
&+\underline{\underline{\vec{A}}}^{01}_{\tau}\cdot\left(-\frac{1}{\sigma_t}\right)\left[\underline{\underline{A}}^{00}_{\tau}\right]^{-1}\sum_{\partial\tau_k\in\partial\tau}\alpha_2\underline{\underline{\vec{A}}}^{00}_{\partial\tau_k}2\underline{\underline{H}}_{\tau}\underline{F}_C\\
&+\underline{\underline{\vec{A}}}^{01}_{\tau}\cdot\left(-\frac{1}{\sigma_t}\right)\left[\underline{\underline{A}}^{00}_{\tau}\right]^{-1}\sum_{\partial\tau_k\in\partial\tau}\alpha_2\underline{\underline{\vec{A}}}^{00}_{\partial\tau_k}2\left(-\underline{F}_D\right)\\
&+\underline{\underline{\vec{A}}}^{01}_{\tau}\cdot\left(-\frac{1}{\sigma_t}\right)\left[\underline{\underline{A}}^{00}_{\tau}\right]^{-1}\underline{\underline{\vec{A}}}^{01}_{\tau}\frac{1}{3}\underline{F}_D\\
&+\sigma_a\underline{\underline{A}}^{00}_{\tau}\underline{F}_D=\sigma_s\underline{\underline{A}}^{00}_{\tau}\left(\underline{\phi}^{(l+1/2)}-\underline{\phi}^{(l)}\right),
\end{aligned} \tag{2.53}$$

And solve for $\underline{F}_D$:

$$\begin{aligned}
&\vec{\underline{\underline{A}}}^{01}_{\tau} \cdot \frac{1}{\sigma_t} \left[\underline{\underline{A}}^{00}_{\tau}\right]^{-1} \left(\sum_{\partial\tau_k \in \partial\tau} 2\alpha_2 \vec{\underline{\underline{A}}}^{00}_{\partial\tau_k} - \frac{1}{3}\vec{\underline{\underline{A}}}^{01}_{\tau} \right) \underline{F}_D \\
&+ \sum_{\partial\tau_k \in \partial\tau} \vec{\underline{\underline{A}}}^{00}_{\partial\tau_k} \cdot 2\vec{\alpha}_{k,1} \underline{F}_D + \sigma_a \underline{\underline{A}}^{00}_{\tau} \underline{F}_D \\
&= \sum_{\partial\tau_k \in \partial\tau} \vec{\underline{\underline{A}}}^{00}_{\partial\tau_k} \cdot 2\vec{\alpha}_{k,1} \underline{\underline{H}}_{\tau} \underline{F}_C \\
&+ \vec{\underline{\underline{A}}}^{01}_{\tau} \cdot \frac{1}{\sigma_t} \left[\underline{\underline{A}}^{00}_{\tau}\right]^{-1} \sum_{\partial\tau_k \in \partial\tau} 2\alpha_2 \vec{\underline{\underline{A}}}^{00}_{\partial\tau_k} \underline{\underline{H}}_{\tau} \underline{F}_C \\
&+ \sigma_s \underline{\underline{A}}^{00}_{\tau} \left(\underline{\phi}^{(l+1/2)} - \underline{\phi}^{(l)} \right),
\end{aligned} \tag{2.54}$$

This operator involves only operations in one element, much like the inversion of the transport operator cell by cell. Once $\underline{F}_D$ has been obtained for every element, we update with the now familiar equation:

$$\underline{\phi}^{(l+1)} = \underline{\phi}^{(l+1/2)} + \underline{F}_D. \tag{2.55}$$

This method, as discussed in the Analysis and Results chapters, behaves similar to a fully consistent DSA scheme for many regimes. However, its performance degrades when the aspect ratio of an element becomes large.

CHAPTER III

ANALYSIS

In this chapter, we will analyze the discussed methods using expansion of iteration error in Fourier modes. It is instructive to detail the analysis of at least one method, the semi-consistent DSA, so the meaning of the results is clearer. These results include two-dimensional eigenvalue maps of spectral radius of the iterative operator, and comparison among methods of the maximum spectral radius of each of these surfaces as a function of cell optical thickness, $\sigma_t h$, for rectangular cells.

A. Fourier Expansion Analysis

In this section, we detail the Fourier expansion and the way we obtain spectral radii from that expansion.

1. Operator Definition

To ease the analysis, we represent the method using operator notation. Operators are denoted by the addition of a chevron over them. Beginning with the discrete transport equation, we define the following operators:

$$\widehat{L} = \sum_{\tau\in\Gamma} \underline{\underline{P}}_{\tau}^{T} \left[\left(- \sum_{\vec{n}_k\cdot\vec{\Omega}<0} \vec{\Omega}\cdot\underline{\underline{\vec{A}}}_{\partial\tau_k}^{00} + \vec{\Omega}\cdot\underline{\underline{\vec{A}}}_{\tau}^{01} + \sigma_t \underline{\underline{A}}_{\tau}^{00} \right) \underline{\underline{P}}_{\tau} + \sum_{\vec{n}_k\cdot\vec{\Omega}<0} \vec{\Omega}\cdot\underline{\underline{\vec{A}}}_{\partial\tau_k}^{00} \underline{\underline{E}}_{\partial\tau_k} \right], \tag{3.1}$$

$$\widehat{K} = \sum_{\tau \in \Gamma} \underline{\underline{P}}_{\tau}^{T} \left[\frac{\sigma_s}{4\pi} \underline{\underline{A}}^{00} \right] \underline{\underline{P}}_{\tau}, \tag{3.2}$$

$$\widehat{M} = \int_{4\pi} d\Omega. \tag{3.3}$$

Here $\underline{\underline{P}}_{\tau}$ is a map from the element space to the global discontinuous space, and $\underline{\underline{E}}_{\partial\tau_k}$ is a map from element space to unknowns in the up-wind cell in global discontinuous space. We use the operator notation to express the discrete transport equation:

$$\widehat{L}\underline{\Psi}^{(l+1/2)}\left(\vec{\Omega}\right) = \widehat{K}\underline{\Phi}^{(l)} + \underline{q}, \tag{3.4}$$

$$\underline{\Phi}^{(l+1/2)} = \widehat{M}\underline{\Psi}^{(l+1/2)}\left(\vec{\Omega}\right). \tag{3.5}$$

Here $\underline{\Psi}^{(l+1/2)}\left(\vec{\Omega}\right)$ is the global list of discontinuous angular intensities, and $\underline{\Phi}^{(l)}$ is the global list of discontinuous scalar intensities. Solving for $\underline{\Phi}^{(l+1/2)}$ in terms of $\underline{\Phi}^{(l)}$:

$$\underline{\Phi}^{(l+1/2)} = \widehat{M}\widehat{L}^{-1}\widehat{K}\underline{\Phi}^{(l)} + \widehat{M}\widehat{L}^{-1}\underline{q}. \tag{3.6}$$

We define another operator:

$$\widehat{A} = \widehat{I} - \widehat{M}\widehat{L}^{-1}\widehat{K}, \tag{3.7}$$

and the source:

$$\underline{b} = \widehat{M}\widehat{L}^{-1}\underline{q}. \tag{3.8}$$

Then as l becomes large, $\underline{\Phi}^{(l)}$ will limit to $\underline{\Phi}^{(l+1/2)}$, and the following equation holds:

$$\widehat{A}\underline{\Phi}^{(l)} = \underline{b}. \tag{3.9}$$

We now define operators for the continuous correction equation:

$$\widehat{B}_C = \sum_{\tau\in\Gamma} \underline{\underline{H}}_\tau^T \left[\sum_{\partial\tau_k\in\partial\Gamma} -\frac{1}{3\sigma_t}\vec{n}_{\partial\tau}\cdot\underline{\underline{\vec{A}}}_{\partial\tau_k}^{01} + \frac{1}{3\sigma_t}\underline{\underline{A}}_\tau^{11} + \sigma_a\underline{\underline{A}}_\tau^{00} \right] \underline{\underline{H}}_\tau \tag{3.10}$$

$$\widehat{K}_C = \sum_{\tau\in\Gamma} \underline{\underline{H}}_\tau^T \sigma_s \underline{\underline{A}}_\tau^{00} \underline{\underline{P}}_\tau \tag{3.11}$$

The continuous correction, $\underline{F}_C$, is then given by:

$$\underline{F}_C = \widehat{B}_C^{-1}\widehat{K}_C\left(\underline{\Phi}^{(l+1/2)} - \underline{\Phi}^{(l)}\right). \tag{3.12}$$

Finally, we define operators for the proposed discontinuous correction equation:

$$\widehat{B}_D = \sum_{\tau\in\Gamma} \underline{\underline{P}}_\tau^T \left[\begin{array}{l} \underline{\underline{\vec{A}}}_\tau^{01}\cdot\dfrac{1}{\sigma_t}\left[\underline{\underline{A}}_\tau^{00}\right]^{-1}\left(\displaystyle\sum_{\partial\tau_k\in\partial\tau} 2\alpha_2\underline{\underline{\vec{A}}}_{\partial\tau_k}^{00} - \frac{1}{3}\underline{\underline{\vec{A}}}_\tau^{01}\right) \\ \quad + \displaystyle\sum_{\partial\tau_k\in\partial\tau} \underline{\underline{\vec{A}}}_{\partial\tau_k}^{00}\cdot 2\vec{\alpha}_{k,1} + \sigma_a\underline{\underline{A}}_\tau^{00} \end{array} \right] \underline{\underline{P}}_\tau, \tag{3.13}$$

$$\widehat{R} = \sum_{\tau\in\Gamma} \underline{\underline{P}}_\tau^T \left[\sum_{\partial\tau_k\in\partial\tau} \underline{\underline{\vec{A}}}_{\partial\tau_k}^{00}\cdot 2\vec{\alpha}_{k,1} + \underline{\underline{\vec{A}}}_\tau^{01}\cdot\frac{1}{\sigma_t}\left[\underline{\underline{A}}_\tau^{00}\right]^{-1}\sum_{\partial\tau_k\in\partial\tau} 2\alpha_2\underline{\underline{\vec{A}}}_{\partial\tau_k}^{00} \right] \underline{\underline{H}}_\tau. \tag{3.14}$$

The scattering operator used in the discontinuous correction equation is the same as the transport scattering operator, $\widehat{K}$. We solve for the discontinuous correction, $\underline{F}_D$:

$$\underline{F}_D = \widehat{B}_D^{-1}\widehat{R}\underline{F}_C + \widehat{B}_D^{-1}\widehat{K}\left(\underline{\Phi}^{(l+1/2)} - \underline{\Phi}^{(l)}\right). \tag{3.15}$$

We now express the next iterate, $\underline{\Phi}^{(l+1)}$, in terms of the previous iterate using the complete iteration/acceleration scheme:

$$\underline{\Phi}^{(l+1)} = \left(\widehat{I}-\widehat{A}\right)\underline{\Phi}^{(l)} + \underline{R} + \left(\widehat{B}_D^{-1}\widehat{R}\widehat{B}_C^{-1}\widehat{K}_C + \widehat{B}_D^{-1}\widehat{K}\right)\left[\left(\widehat{I}-\widehat{A}\right)\underline{\Phi}^{(l)} - \underline{\Phi}^{(l)}\right]. \tag{3.16}$$

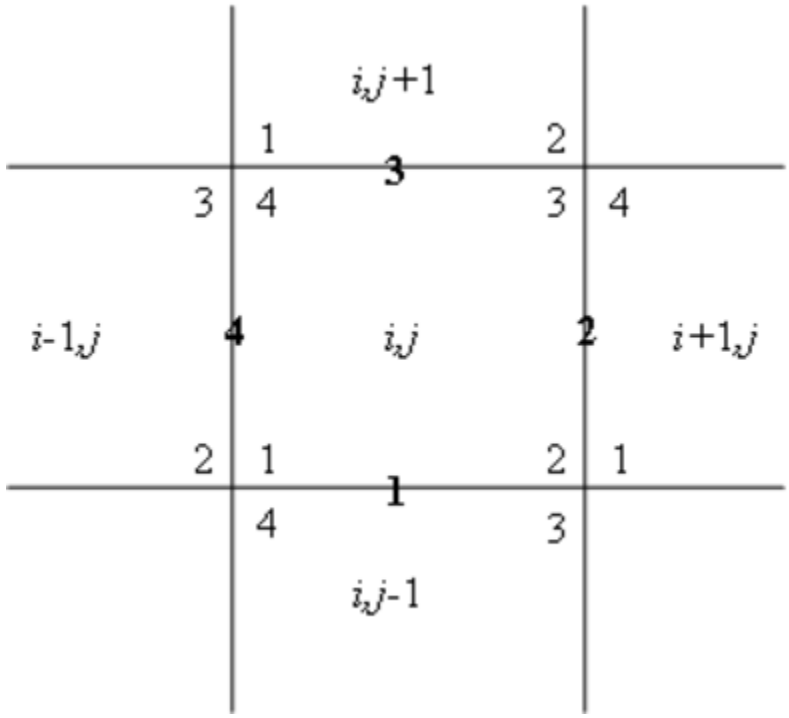

Fig. 2. Reference element of a discontinuous element in the spatial mesh.

This may be expressed as a preconditioned Richardson iteration scheme with preconditioner $\widehat{P}$:

$$\underline{\Phi}^{(l+1)} = \left(\widehat{I} - \widehat{P}\widehat{A}\right)\underline{\Phi}^{(l)} + \underline{b}, \tag{3.17}$$

$$\widehat{P} = \widehat{I} + \widehat{B}_D^{-1}\left(\widehat{R}\widehat{B}_C^{-1}\widehat{K}_C + \widehat{K}\right). \tag{3.18}$$

The identification of the preconditioner allows implementation as part of a Krylov iteration. Defining the Fourier expansion of these operators allows us to find the spectral radii simply and symbolically.

2. Fourier Expansion

We will now detail modifications to the above operators when the iterates are expanded in the Fourier modes. To do so, we must first define our problem and the Fourier ansatz it allows us to make. We choose a steady state, mono-energetic, 2-D infinite-homogeneous-medium with scattering ratio defined by c, and constant extraneous source. For the DFEM matrices, we choose either PWLD or BLD matrices. We choose a grid of regular-rectangular elements. We introduce the discontinuous reference element in Fig. (2). The index to unknowns is given by normal script numbers; face numbering is given by bold numbers; element indicies are given by pairs of italicized numbers (or in this case, letters).

We seek equations for the iteration error given by our method, which we denote with an asterisk:

$$\underline{\Phi}_{*}^{(l)} = \underline{\Phi}^{(l)} - \underline{\Phi}. \tag{3.19}$$

In our infinite-medium model problem, the eigenfunctions of our operators are Fourier modes. It therefore facilitates our analysis to expand the iteration error spatially in Fourier series. We denote Fourier coefficients with a dagger:

$$\underline{\phi}_{*,\tau}^{(l)} = \omega^{l} \underline{\underline{P}}_{\tau}^{\dagger} \underline{\Phi}^{\dagger}, \tag{3.20}$$

with:

$$\underline{\underline{P}}_{\tau}^{\dagger} = \underline{\underline{P}}_{\tau} e^{i\sigma_t \vec{\lambda}\cdot\vec{r}_{\tau}}. \tag{3.21}$$

Here $\lambda = (\lambda_x, \lambda_y)$, where λ_x and λ_y are proportional to the frequencies of the error mode along the x and y axes, respectively. Each λ can range from $-\infty$ to $+\infty$. We choose $\vec{r}_{\tau}$ to be taken at the bottom left corner of the rectangular element τ. It is

also necessary to expand the continuous correction in Fourier modes:

$$\underline{F}_C = \omega^l \underline{\underline{H}}^\dagger_\tau F^\dagger_C, \tag{3.22}$$

with:

$$\underline{\underline{H}}^\dagger_\tau = \begin{pmatrix} e^{i\sigma_t \vec{\lambda}\vec{r}_{i,j}} & 0 & 0 & 0 \\ 0 & e^{i\sigma_t \vec{\lambda}\vec{r}_{i+1,j}} & 0 & 0 \\ 0 & 0 & e^{i\sigma_t \vec{\lambda}\vec{r}_{i+1,j+1}} & 0 \\ 0 & 0 & 0 & e^{i\sigma_t \vec{\lambda}\vec{r}_{i,j+1}} \end{pmatrix} \underline{\underline{H}}_\tau \tag{3.23}$$

We will now describe the simplification the Fourier expansion of unknowns allows. The operator $\widehat{L}$ couples all elements together through the up-wind map. We define the up-wind maps (one per face) which incorporate the Fourier expansion of spatial

location:

$$\underline{\underline{E}}^{\dagger}_{\partial\tau_k} = \begin{cases} \begin{pmatrix} 0 & 0 & 0 & 1 \\ 0 & 0 & 1 & 0 \\ 0 & 0 & 0 & 0 \\ 0 & 0 & 0 & 0 \end{pmatrix} e^{i\sigma_t \vec{\lambda}\vec{r}_{\partial\tau_k^+}} & k = 1 \\ \begin{pmatrix} 0 & 0 & 0 & 0 \\ 1 & 0 & 0 & 0 \\ 0 & 0 & 0 & 1 \\ 0 & 0 & 0 & 0 \end{pmatrix} e^{i\sigma_t \vec{\lambda}\vec{r}_{\partial\tau_k^+}} & k = 2 \\ \begin{pmatrix} 0 & 0 & 0 & 0 \\ 0 & 0 & 0 & 0 \\ 0 & 1 & 0 & 0 \\ 1 & 0 & 0 & 0 \end{pmatrix} e^{i\sigma_t \vec{\lambda}\vec{r}_{\partial\tau_k^+}} & k = 3 \\ \begin{pmatrix} 0 & 1 & 0 & 0 \\ 0 & 0 & 0 & 0 \\ 0 & 0 & 0 & 0 \\ 0 & 0 & 1 & 0 \end{pmatrix} e^{i\sigma_t \vec{\lambda}\vec{r}_{\partial\tau_k^+}} & k = 4 \end{cases} . \tag{3.24}$$

It is necessary to mention that when we take the transpose of the maps $\underline{\underline{P}}^{\dagger}_{\tau}$, $\underline{\underline{H}}^{\dagger}_{\tau}$, or $\underline{\underline{E}}^{\dagger}_{\partial\tau_k}$, we use the Hermite transpose, resulting in the complex conjugate of the matrix or vector. We then define transport operators using the redefined Fourier maps; we do this by replacing the maps listed above with their Fourier model counterparts,

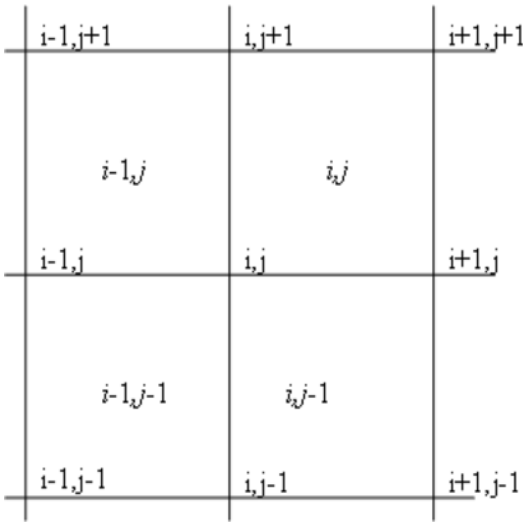

Fig. 3. Nine-point stencil for vertex (i,j) of a continuous finite element.

e.g.:

$$\widehat{L}^{\dagger} = \sum_{\tau \in \Gamma} \underline{\underline{P}}_{\tau}^{\dagger T} \left[\left(- \sum_{\vec{n}_k \cdot \vec{\Omega} < 0} \vec{\Omega} \cdot \underline{\underline{\vec{A}}}_{\partial \tau_k}^{00} + \vec{\Omega} \cdot \underline{\underline{\vec{A}}}_{\tau}^{01} + \sigma_t \underline{\underline{A}}_{\tau}^{00} \right) \underline{\underline{P}}_{\tau}^{\dagger} + \sum_{\vec{n}_k \cdot \vec{\Omega} < 0} \vec{\Omega} \cdot \underline{\underline{\vec{A}}}_{\partial \tau_k}^{00} \underline{\underline{E}}_{\partial \tau_k}^{\dagger} \right], \tag{3.25}$$

$$\widehat{A}^{\dagger} = \widehat{I} - \widehat{M} \widehat{L}^{\dagger - 1} \widehat{K}^{\dagger}. \tag{3.26}$$

The operator $\widehat{A}^{\dagger}$ is an infinite block diagonal matrix with each block identical to the other blocks. Thus, we only need to evaluate the block corresponding to one arbitrary element to fully solve the system.

The CFEM involves the nearest nine neighbors for each row of the global matrix. In Figure 3 we introduce the nine point stencil for the equation for the unknown at one vertex of the continuous correction equation. Element indices are given by pairs of italicized integers, and unknowns at vertices are denoted by pairs of non-italicized integers. We find the equation for the Fourier expanded correction at vertex (i,j)

by taking a summation of the matrices of the four elements that share vertex (i,j). The result is a 9x9 matrix, with only the row corresponding to vertex (i,j) having all contributing elements accounted for. We may reduce this matrix to a 1x1 problem at vertex (i,j) because each continuous Fourier mode has one degree of freedom. We do this by only using the row of $\underline{\underline{H}}_{\tau}^{\dagger}$ associated with vertex (i,j). We then use this fact again to find the value at the other vertices in element τ. We define continuous operators using the reduced maps:

$$\widehat{B}_C^{\dagger} = \sum_{\tau_{i,j} \;\; at \;\; (i,j)} \left(\underline{H}_{(i,j)}^{\dagger T} \frac{1}{3\sigma_t} \underline{\underline{\tilde{A}}}_{\tau}^{11} + \sigma_a \underline{\underline{A}}_{\tau}^{00} \right) \underline{H}_{(i,j)}^{\dagger}, \tag{3.27}$$

$$\widehat{K}_C^{\dagger} = \sum_{\tau_{i,j} \;\; at \;\; (i,j)} \underline{H}_{i,j}^{\dagger T} \sigma_s \underline{\underline{A}}_{\tau}^{00} \underline{\underline{P}}_{\tau}^{\dagger}. \tag{3.28}$$

For the 2-D rectangular model problem $\widehat{B}_C$ is 1x1, and $\widehat{K}_C$ is 1x4 in dimension. We write the equation for the Fourier coefficient for the continuous correction in operator notation:

$$\omega^l \widehat{B}_C^{\dagger} F_C^{\dagger} = \omega^l \widehat{K}_C^{\dagger} \left(\left[\widehat{I} - \widehat{A}^{\dagger} \right] - \widehat{I} \right) \underline{\Phi}^{\dagger}. \tag{3.29}$$

We solve Eq. (3.29) for $F_C^{\dagger}$:

$$F_C^{\dagger} = \widehat{B}_C^{\dagger -1} \widehat{K}_C^{\dagger} \left(-\widehat{A}^{\dagger} \right) \underline{\Phi}^{\dagger}. \tag{3.30}$$

We now define corresponding operators from the proposed DSA section:

$$\widehat{B}_D^{\dagger} = \sum_{\tau \in \Gamma} \underline{\underline{P}}_{\tau}^{\dagger T} \left[\begin{array}{l} \vec{\underline{\underline{A}}}_{\tau}^{01} \cdot \frac{1}{\sigma_t} \left[\underline{\underline{A}}_{\tau}^{00} \right]^{-1} \left(\sum_{\partial\tau_k \in \partial\tau} 2\alpha_2 \vec{\underline{\underline{A}}}_{\partial\tau_k}^{00} - \frac{1}{3} \vec{\underline{\underline{A}}}_{\tau}^{01} \right) \\ + \sum_{\partial\tau_k \in \partial\tau} \vec{\underline{\underline{A}}}_{\partial\tau_k}^{00} \cdot 2\vec{\alpha}_{k,1} + \sigma_a \underline{\underline{A}}_{\tau}^{00} \end{array} \right] \underline{\underline{P}}_{\tau}^{\dagger}, \tag{3.31}$$

$$\widehat{R} = \sum_{\tau \in \Gamma} \underline{\underline{P}}_{\tau}^{\dagger T} \left[\sum_{\partial\tau_k \in \partial\tau} \vec{\underline{\underline{A}}}_{\partial\tau_k}^{00} \cdot 2\vec{\alpha}_{k,1} + \vec{\underline{\underline{A}}}_{\tau}^{01} \cdot \frac{1}{\sigma_t} \left[\underline{\underline{A}}_{\tau}^{00} \right]^{-1} \sum_{\partial\tau_k \in \partial\tau} 2\alpha_2 \vec{\underline{\underline{A}}}_{\partial\tau_k}^{00} \right] \underline{\underline{H}}_{\tau}^{\dagger}. \tag{3.32}$$

After substituting the expression for $F_C^\dagger$, the equation for the Fourier coefficient of the discontinuous correction is:

$$\widehat{B}_D^\dagger \underline{F}_D^\dagger = \widehat{K}^\dagger \left(\left[\widehat{I} - \widehat{A}^\dagger \right] - \widehat{I} \right) \underline{\Phi}^\dagger + \widehat{R}^\dagger \widehat{B}_C^{\dagger -1} \widehat{K}_C^\dagger \left(\left[\widehat{I} - \widehat{A}^\dagger \right] - \widehat{I} \right) \underline{\Phi}^\dagger \tag{3.33}$$

Finally, the update equation becomes:

$$\omega \underline{\Phi}^\dagger = \left(\widehat{I} - \widehat{A}^\dagger \right) \underline{\Phi}^\dagger + \widehat{B}_D^{\dagger -1} \widehat{K}^\dagger \left(-\widehat{A}^\dagger \right) \underline{\Phi}^\dagger + \widehat{B}_D^{\dagger -1} \widehat{R}^\dagger \widehat{B}_C^{\dagger -1} \widehat{K}_C^\dagger \left(-\widehat{A}^\dagger \right) \underline{\Phi}^\dagger \tag{3.34}$$

or,

$$\omega \underline{\Phi}^\dagger = \left(\widehat{I} - \widehat{P}^\dagger \widehat{A}^\dagger \right) \underline{\Phi}^\dagger, \tag{3.35}$$

with:

$$\widehat{P}^\dagger = \widehat{I} + \widehat{B}_D^{\dagger -1} \left(\widehat{K}^\dagger + \widehat{R}^\dagger \widehat{B}_C^{\dagger -1} \widehat{K}_C^\dagger \right). \tag{3.36}$$

We may see then that the eigenvalues, ω, are the eigenvalues of the preconditioned operator. In the next section, we discuss these eigenvalues and compare them to those of unaccelerated transport and the inconsistent DSA methods discussed in the previous section.

B. Properties of Proposed DSA Method

In this section we display spectral maps of the iteration operator defined in the previous section, namely $\left(\widehat{I} - \widehat{P}^\dagger \widehat{A}^\dagger \right)$, for a set of model problems that illustrate the important characteristics of our method. Note that for a given mode (characterized by $\vec{\lambda}$), the operators contain sine and cosine functions of θ_x and $\sigma_t \lambda_y \Delta y$, where:

$$\theta_x = \sigma_t \lambda_x \Delta x, \tag{3.37}$$

$$\theta_y = \sigma_t \lambda_y \Delta y. \tag{3.38}$$

That is, the operators are periodic in these quantities. These maps are made by finding the maximum-magnitude eigenvalue for a value of (θ_x, θ_y) in the Fourier expansion. In 2-D, these values are in the space $(-\infty, -\infty)$ to (∞, ∞)); however, the operator is periodic from $(0, 0)$ to $(2\pi, 2\pi)$, and reflected about $(0, 0)$ to (π, π). We make maps for various cell optical thicknesses in the x direction, $\sigma_t \Delta x$, and y direction, $\sigma_t \Delta x$.

Figure 4 shows the spectral radii over Fourier-modes of interest for a small sample of cell geometries. For thin cells (optical thicknesses much less than 1 mfp), the spectral radius remains small. As the cell optical thickness increases to the order of 1-10 mfp, the spectral radius increases and, as aspect ratio increases, approaches the scattering ratio, c. As cell optical thickness becomes large, the spectral radius decreases, though it is larger for larger aspect ratios.

It is interesting to note several phenomena. The rays, which are most visible in cells with optical thickness .001 mfp, are caused by the quadrature set (S_4) used to evaluate angular integrals. If we increase degree of the quadrature set, we increase the number of rays. These rays merge as aspect ratio increases. The maximum spectral radius occurs along these rays, and for low-frequency modes (θ_x, θ_y is small). For cells with optical thickness on the order of 1-10 mfp, the maximum spectral radius occurs for low frequency modes of θ_x. However, for cells with optical thickness much greater than 1 mfp, the maximum occurs for high-frequency modes. As cells become very large, the spectral radius decreases for all modes.

In the next section, we use discuss the maximum spectral radius of the proposed DSA method for varying cell optical thicknesses and aspect ratios. We also compare spec-

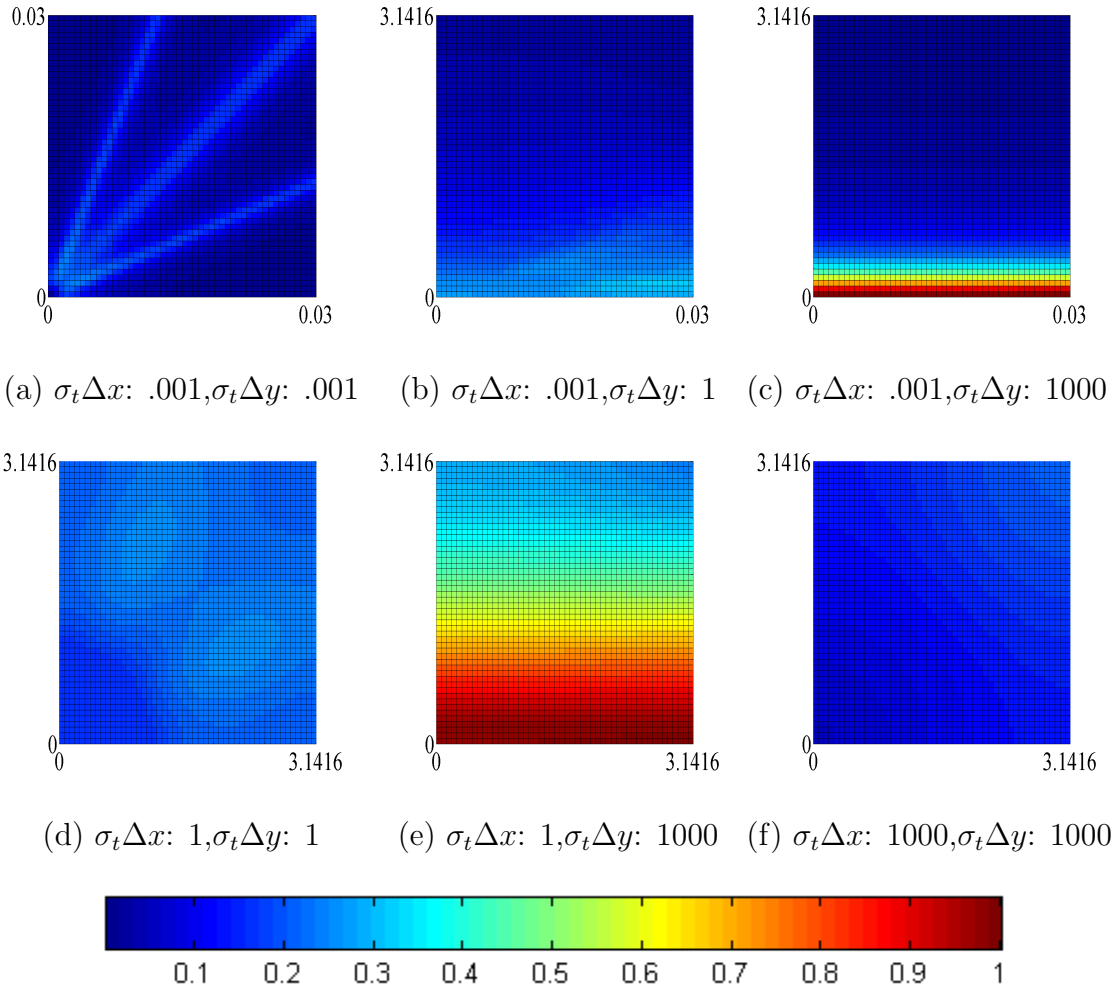

(a) $\sigma_t\Delta x$: .001,$\sigma_t\Delta y$: .001 (b) $\sigma_t\Delta x$: .001,$\sigma_t\Delta y$: 1 (c) $\sigma_t\Delta x$: .001,$\sigma_t\Delta y$: 1000

(d) $\sigma_t\Delta x$: 1,$\sigma_t\Delta y$: 1 (e) $\sigma_t\Delta x$: 1,$\sigma_t\Delta y$: 1000 (f) $\sigma_t\Delta x$: 1000,$\sigma_t\Delta y$: 1000

Fig. 4. Spectral radii for Fourier modes with $c = .99$. Graph axes are θ_x and θ_y for the abcissa and ordinate respectively.

tral radii of the proposed DSA method to unaccelerated iteration and an inconsistent, continuous DSA method.

C. Method Comparison

In this section we compare the maximum spectral radii over all modes for unaccelerated transport, inconsistent DSA, and the proposed DSA. We make these comparisons for various cell optical thicknesses and cell aspect ratios.

We begin by comparing line plots of maximum spectral radius with variable aspect ratio, holding scattering ratio constant ($c = .99$). In the figures, normalized spectral radius means the maximum spectral radius divided by the scattering ratio, making figures with different scattering ratios more easily comparable.

Figure 5 shows normalized spectral radius from the Fourier analysis for cells defined by various horizontal mfp from 10^{-3} to 10^{3} and aspect ratios of Fig. 5(a): 1 and Fig. 5(b): 100. Figure 5(c) is a contour plot of the maximum spectral radius of the proposed DSA method over a range of mfp from 10^{-3} to 10^{5} in the x and y directions. The two line plots are two dimensional, diagonal slices of the contour plot. These results are for the Piecewise Linear Discontinuous (PWLD) finite element method.

Next we compare line plots for increasing scattering ratio holding aspect ratio constant at 1. We can see in Fig. 6 the maximum spectral radius degrades over a larger range of cell optical thickness as the scattering ratio approaches unity. This is important to note, as problems of interest frequently have scattering ratios near unity, and may have optical thicknesses spanning many orders of magnitude. It is also important because we can see that it does not affect the value of maximum spectral radius for

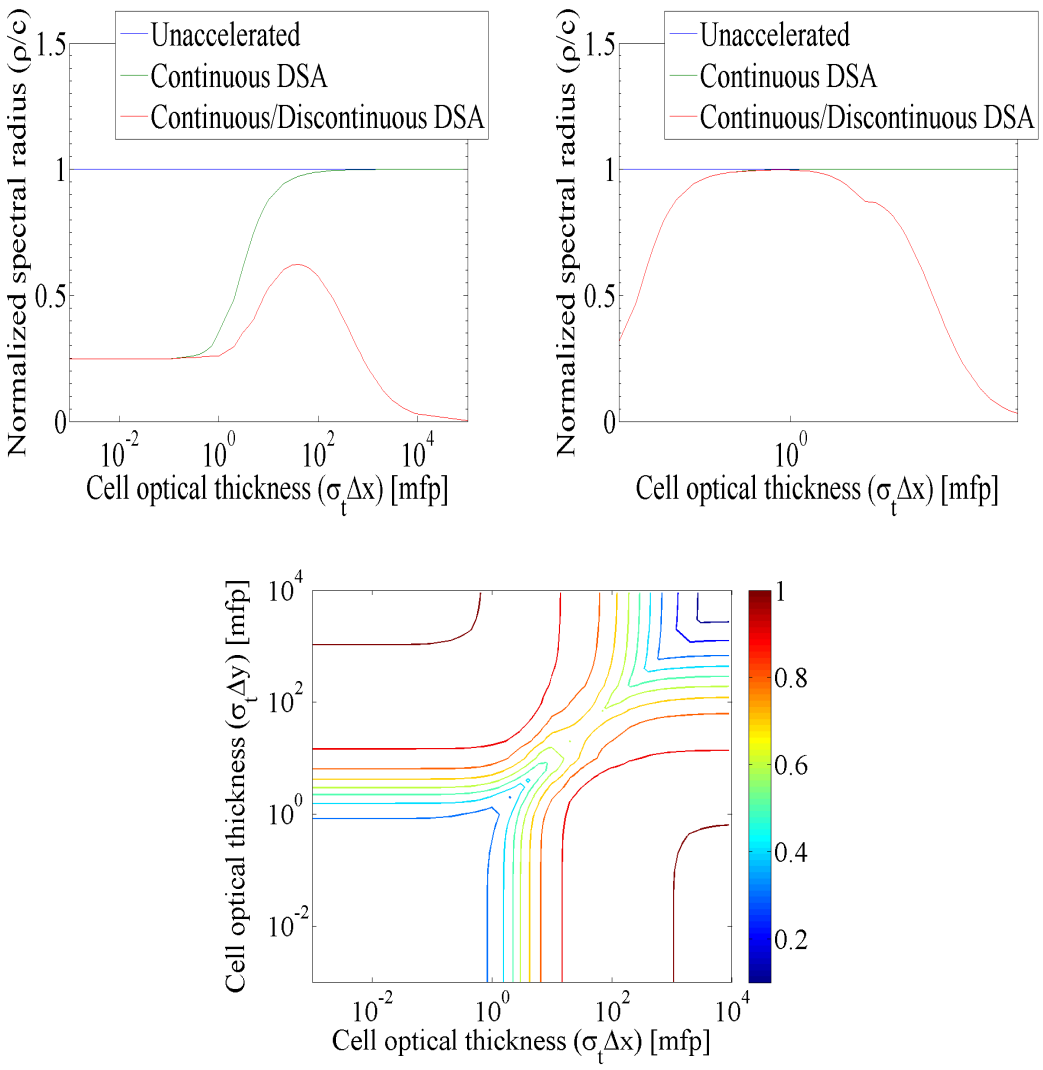

Fig. 5. Maximum normalized spectral radii for Fourier analysis for scattering ratio, c, of .99, with cell optical thickness: $\sigma_t \Delta x$ from 10^{-3} to 10^3, aspect ratio $\Delta y/\Delta x$ (a) 1, and (b) 1000. (c) Maximum spectral radii for $\sigma_t \Delta x$ from 10^{-3} to 10^3 and $\sigma_t \Delta y$ from 10^{-3} to 10^3.

a given aspect ratio; because of this we limit further study to scattering ratios of .99. For cells with low aspect ratio, accelerated iteration with the proposed method does provide a spectral radius reduction regardless of the scattering ratio of the problem.

In Figure 7 we compare the method when used with a PWLD basis, the stiffness matrix approximation, and a BLD basis. The stiffness approximation does not significantly affect the spectral radius of the method. The BLD and PWLD bases provide similar results.

Our results are similar to those observed by Wareing *et al.* [4]. This is as expected and hoped, for the goal was to create generalization of their method to a wider class of DFEMs, geometries, and grid types. In particular, the Fourier analysis predicts excellent performance for square cells but degraded performance for some cells with high aspect ratios, which limits to the scattering ratio for cells with very high aspect ratios. Previous work has shown that using the operator of Wareing *et al.* as a preconditioner within a Krylov iteration performs well even with with high aspect ratio [8].

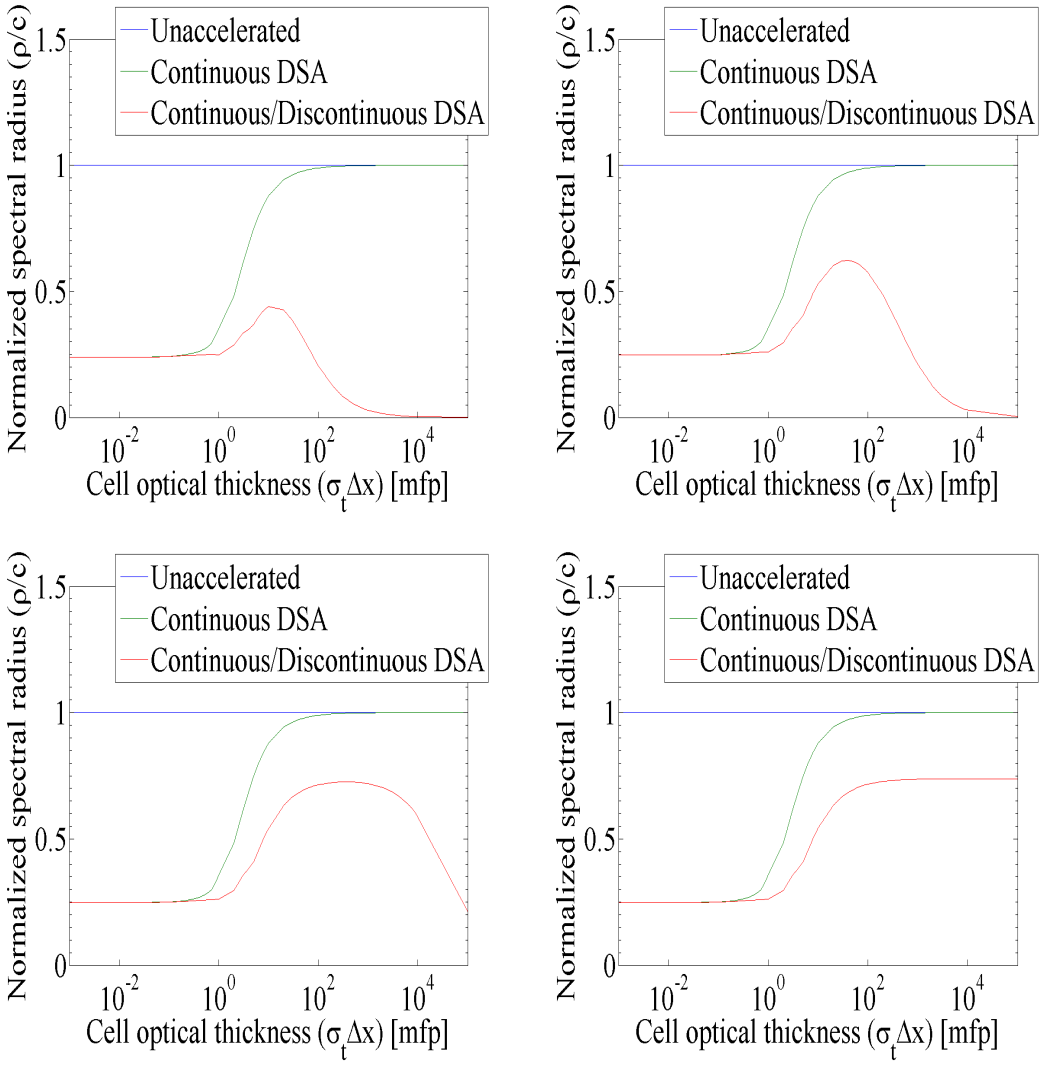

Fig. 6. Maximum normalized spectral radii for aspect ratio of 1 (square cells) with $\sigma_t \Delta x$ from 10^{-3} to 10^3, with $c =$ (a).9, (b).99, (c).9999, (d).99999999.

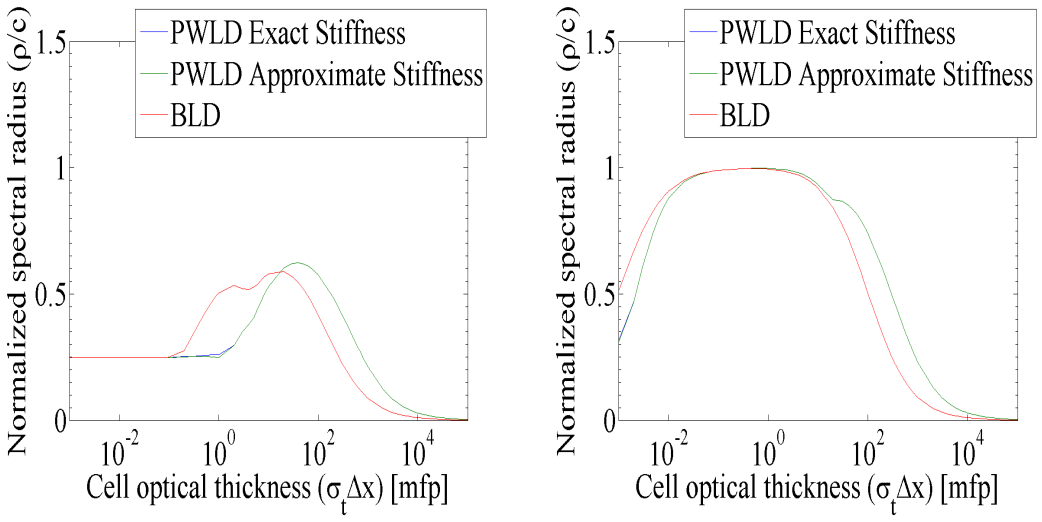

Fig. 7. Maximum normalized spectral radii $\sigma_t \Delta x$ from 10^{-3} to 10^{3} of the PWLD, PWLD with stiffness approximation, and BLD bases for aspect ratios of (a)1, (a)1000.

CHAPTER IV

IMPLEMENTATION AND TESTING

In this chapter we discuss the implementation of the proposed DSA method and numerical results using the proposed DSA method. We choose a set of test problems which have been shown to be of interest; if a method performs well for these test problems, it is a strong indicator that it will perform well for other difficult problems. To analyze the spectral radius of the method, we investigate problems which emulate the Fourier model problem. This investigation was performed with a prototype implementation into MATLAB. We also investigate a problem known to degrade the Wareing method, a periodic horizontal interface (PHI).[9] We then describe test problems run with PDT, a parallel transport code at Texas A&M, which test our method in different geometries and with different finite elements.

A. Simple Test Problems

The goal of the simple test problems is to verify our Fourier analysis. Thus, we choose a test problem to mimic the as closely as possible the model problems we analyzed: we choose a homogeneous medium, isotropic scattering problem with the same scattering ratio and material properties. Furthermore, we choose a vacuum boundary and zero source such that the correct solution is exactly zero. Choosing a non-zero initial guess makes a non-zero error, which, after iteration, should reduce in magnitude by the spectral radius every iteration. Thus, the error is the norm of the current solution, and after many iterations the spectral radius is the ratio of the current iteration error to the previous iteration error.

We attempt to make the problem optically thick so that neutron leakage is a small quantity. However, to make the entire problem optically thick and have optically thin cells simultaneously would require a prohibitive number of cells. Thus, leakage becomes a dominant factor of loss for the optically thin-cell test problems, and the spectral radius of the operator is reduced dramatically. We use problems which are 20 by 20 cells (400 cells, 1600 discontinuous unknowns, 441 vertices, 441 continuous unknowns). We use the Richardson iteration scheme to obtain consecutive estimate the spectral radius of the operator by taking the ratio of the residual calculated at the current iteration to the residual calculated at the previous iteration:

$$\underline{\rho}^l \approx \frac{\underline{r}^l}{\underline{r}^{l-1}} \tag{4.1}$$

The number we report in the figures is the estimated spectral radius once the value has stabilized and changes between consecutive spectral radius estimations is below some user chosen tolerance, 10E-6. It is interesting and useful to note that the spectral radius estimation converges much faster than the residual to the problem; since we were not interested in the solution to the problem, we stopped iteration after the spectral radius estimation converged.

Figure 8 shows normalized spectral radius of the test-problem operator for mfp from .001 to 1000 and cells defined by an aspect ratio of 1 and 100. Figure 8(c) is a contour plot of spectral radius over a range of mfp from 10^{-3} to 10^3 and aspect ratios of 1 to 1000. These results are from the PWLD method. The results for BLD are similar.

We see that except for the thin-cell problems with significant leakage, the results from numerical test problems agree very closely with the results from the Fourier analysis. This gives us confidence that the analysis thus far has been correct. With the 2D transport code we examine a well known flaw with DSA methods: the periodic hori-

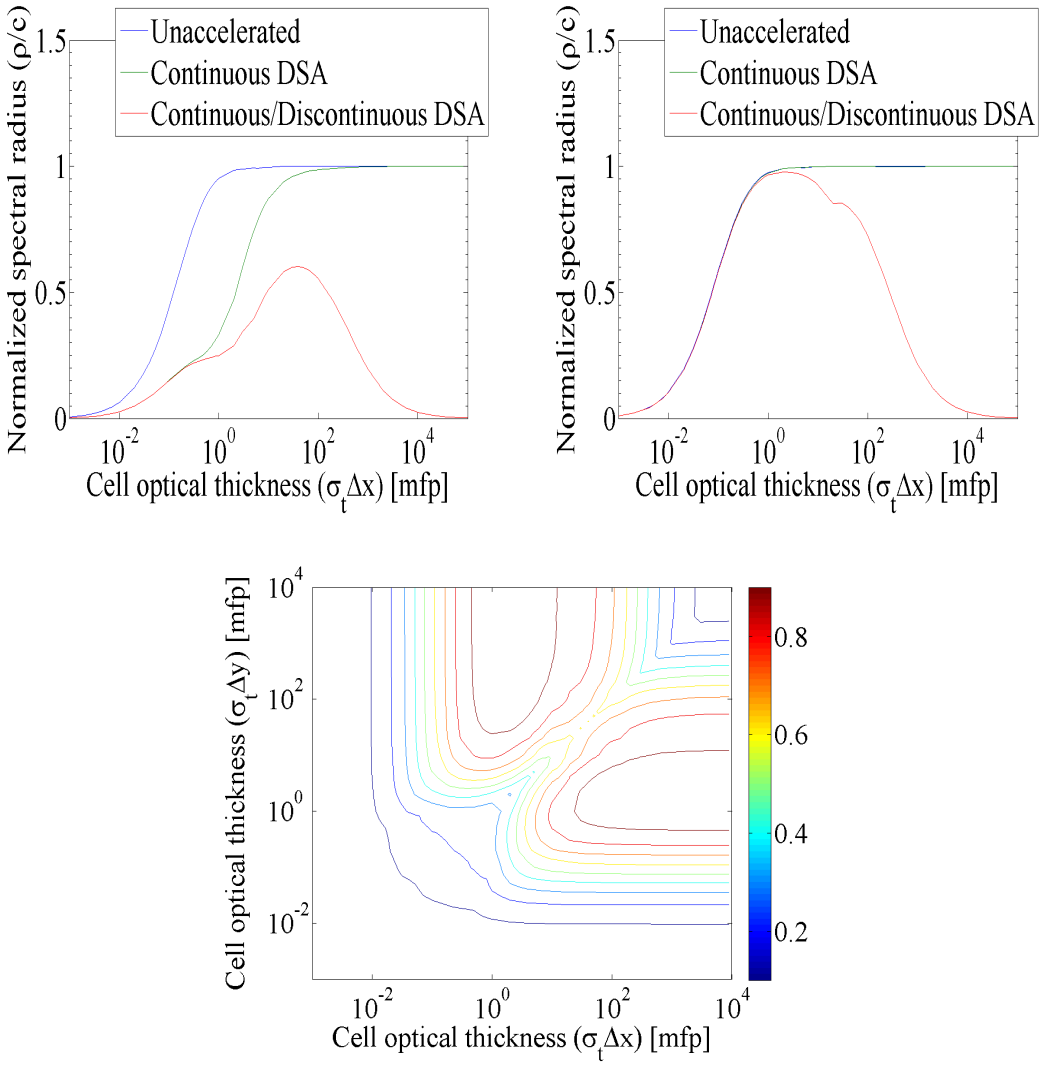

Fig. 8. Maximum normalized spectral radii for homogeneous test problems for scattering ratio, c, of .99, with cell optical thickness: $\sigma_t \Delta x$ from 10^{-3} to 10^3, aspect ratio $\Delta y / \Delta x$ (a) 1, and (b) 1000. (c) Maximum spectral radii for $\sigma_t \Delta x$ from 10^{-3} to 10^3 and $\sigma_t \Delta y$ from 10^{-3} to 10^3.

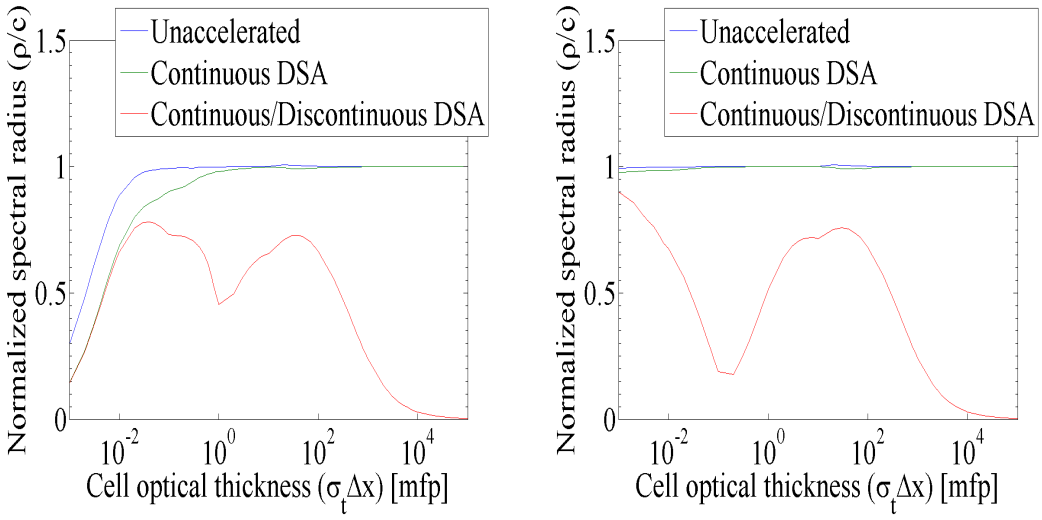

Fig. 9. Maximum spectral radii for PHI test problems for scattering ratio, c, of .99, aspect ratio 1, with cell optical thickness: $\sigma_t \Delta x$ from 10^{-3} to 10^3, and cell optical thickness ratios of (a) 100, and (b) 10000.

zontal interface (PHI) problem. This problem causes difficulty because the diffusion approximation, a P_1 angular approximation to the transport equation, is not valid when there are large material discontinuities. The PHI problem exaggerates this by having multiple discontinuities in the same direction. We describe the PHI problem by cell optical thicknesses for two types of cells, $\sigma_{t,1}\Delta x_1$ and $\sigma_{t,2}\Delta x_2$. We use a scattering ratio of .99, and investigate over cell optical thickness from 10^{-3} to 10^3. We can see in Fig. 9 the spectral radius of the method is increased when compared to homogeneous problems.

B. Grey Radiation Transport Acceleration

When we implemented the method into PDT, this allowed several new abilities for testing our method and for PDT. For our method to work, it requires a diffusion

operator. The diffusion operator of choice operates on a CFEM mesh to obtain a continuous correction, and then performs an additional step to apply the correction to the discontinuous grid. Additionally, we adapted our method to radiative transfer, using a group homogenization scheme developed by Larsen[10]. The homogenization scheme attempts to set the error in the transport equation to zero if the error function has the shape associated with the slowest converging Fourier error modes in frequency space:

$$s_0(\nu) = \frac{\chi(\nu)}{\sigma(\nu) + \tau}, \tag{4.2}$$

$$s_1(\nu) = \frac{\chi(\nu)}{(\sigma(\nu) + \tau)^2}. \tag{4.3}$$

Larsen then used these shape functions to obtain averaged cross sections which guarantee the error for the slowest converging Fourier modes is zero. These cross sections are defined as:

$$\hat{\sigma} = \frac{\int d\nu \sigma_t s_0(\nu)}{\int d\nu s_0(\nu)}, \tag{4.4}$$

$$\hat{\sigma}_T = \frac{\int d\nu s_0(\nu)}{\int d\nu s_1(\nu)}, \tag{4.5}$$

$$\hat{\sigma}_a = \hat{\sigma} * (1 - \eta) + \tau. \tag{4.6}$$

In our diffusion equation, we use:

$$\sigma_t \leftarrow \hat{\sigma}, \tag{4.7}$$

$$D \leftarrow \frac{1}{3\hat{\sigma}_T} \tag{4.8}$$

Table I. PDT iterations to converge the homogeneous test problems with c=0.9999. (Unaccelerated, continuous diffusion, proposed)

$\sigma_t\Delta y \backslash \sigma_t\Delta x$	0.1	1	10	100	1000
0.1	19 15 15				21 13 13
1		283 13 12		283 76 71	394 142 130
10			1933 28 16		1552 200 83
100				283 34 19	336 107 38
1000					52 31 20

$$\sigma_a \leftarrow \hat{\sigma}_a \tag{4.9}$$

C. PDT Test Problems

The first test problems are analogous to the simple test problems, but with more cells so that iteration operators are not strongly dominated by leakage for optically thin problems. We use the stiffness approximation discussed in Chapter II. We use the GMRES Krylov method for solving both the transport DFEM and the diffusion CFEM. Because the diffusion operator is symmetric positive definite, a better algorithm, such as conjugate gradient, could be used for the diffusion solution. We compare GMRES iterations between unaccelerated, CFEM DSA, and the proposed DSA. For the following problems we used one group, 40 by 40 cells, and we used the unlumped PWLD FEM in two dimensions, with scattering ratio of 0.9999. Unaccelerated iteration is in normal text, acceleration with a continuous diffusion correction is in italics, and the proposed acceleration method is in bold.

Table II. Iterations to converge the continuous diffusion correction for homogeneous test problems with c=0.9999.

$\sigma_t\Delta y \backslash \sigma_t\Delta x$	0.1	1	10	100	1000
0.1	688				4832
1		362		1385	1883
10			410		840
100				54	160
1000					62

The iteration results agree with test results: problems with larger scattering ratios take more iterations to converge, and problems with higher aspect ratios take more iterations to converge. We can see that the continuous DSA reduces iterations, and the proposed DSA method reduces more. Although the iterations were reduced, the runtime to solution was not. This is because the continuous diffusion correction was solved to the same tolerance as the transport equation. In practice, it is not always beneficial to solve the correction to such a tight tolerance. Table II shows how many GMRES iterations were necessary to find the continuous diffusion correction at each transport iteration step. We notice that the number of iterations increases as the aspect ratio of the cells increases, but decreases as the cell optical thickness increases. For future work, we will need devise a scheme which will choose an appropriate tolerance for the diffusion CFEM correction, and to precondition the acceleration method using a multigrid method.

CHAPTER V

CONCLUSION

A. Summary

Our motivation for this thesis was to develop a transport equation acceleration method which had adequate performance, particularly in the thick and thin cell limits. We also wanted the method to be implemented without the need to define new matrices or allocate additional storage for cell matrices, and have the flexibility to use an arbitrary finite element method.

We took inspiration from Wareing's accelerator for the bilinear DFEM, and generalized the equations to be applicable to any finite element method. Additionally, we derived an approximation to the stiffness matrix using matrices already defined in the finite element transport equation. This eliminated any need for additional matrices to be defined or stored.

To determine the performance of the method, we determined the operator spectral radius of the method using Fourier analysis, and with model problems in MATLAB. We found that the analysis agreed with the model problem results, and that performance was adequate in the thick and thin cell limits. We also determined that the method performance was dependent on the aspect ratio of cells used, limiting to the scattering ratio as aspect ratio increased. There was not a significant difference in operator spectral radius when using either the stiffness matrix or the derived approximation to the stiffness matrix, or when using a PWLD or BLD basis. We also tested a periodic heterogeneous interface (PHI) problem in MATLAB, and found the method degrades

over a larger range as the ratios of optical thickness between cells increases. This phenomenon has been documented for many other diffusion accelerators. However, the thick and thin cell limits maintained good performance.

Using the transport code PDT we determined iterations to convergence with the GMRES iterative algorithm. The iteration results agree with analysis predictions and are consistent with MATLAB results from simple test problems. In all cases, the accelerator decreases the number of transport iterations significantly. We showed the proposed accelerator decreases the iterations more than a CFEM diffusion correction in the thick cell limit, but behaves similarly in the thin cell limit. Since the proposed method only requires an additional calculation per cell and provides a significant increase over the CFEM acceleration method, its improved performance comes at almost no computational cost.

For our simple test problems with our current implementation the total run time increased. This was because the simple test problems did not have many quadrature directions or energy groups; also the continuous diffusion correction used in both accelerators was converged to the same tolerance as the transport problem. In practice, the transport operation should be expensive compared to obtaining a one-group (grey) diffusion solution. Finding the optimal tolerance for the correction problem is problem dependent, and was not done as part of our evaluation of the iterative performance of either acceleration method. We recommend that strategies for varying the iterative tolerance in the diffusion solution be developed in future work.

The method was found to meet our criteria: it supports arbitrary FEM, as shown by some example problems using the PWLD and BLD bases functions; it performs well in thick and thin cell problems, as shown by Fourier analysis as well as test problems

executed by both MATLAB and PDT; it does not require additional FEM matrix definition by the user, keeping the memory requirement to a minimum necessary to solve an iterative algorithm for the continuous diffusion correction; and it permits a DSA implementation that is independent of the details of the underlying FEM.

B. Future Work

The speed and memory requirements of using the diffusion preconditioner in PDT need to be improved. There are several promising avenues to pursue for this. One is to use a conjugate gradient method, which will improve speed and memory usage of the diffusion solution procedure. However, even with a conjugate gradient solver, we know that we will ultimately need a preconditioner for the CFEM diffusion equation that scales well to large problems on large parallel machines. Some form of multigrid will probably be the only option for meeting this requirement. If we are willing to store some matrices in each cell, it is possible to calculate each cell's contribution to the grey CFEM diffusion operator only once per change in cell material properties. As a project for PDT specifically, we will need to change how calculation and storage of unknowns is performed. Currently, unknowns are being stored on each cell and on a distributed parallel data-structure supplied by the Parasol group at Texas A&M (PTTL/STAPL).

We suggest developing heuristics for finding a reasonable tolerance which to converge the continuous diffusion correction. How tightly to converge the accelerator solution is difficult for a user to know *a priori*. The optimal tolerance may be material property dependent, which can change over time steps.

We will want to investigate other geometry configurations, particularly cylindrical and spherical geometries, and how they will affect the approximations we chose at interfaces. It would be instructional to do the Fourier analysis of the proposed method in 3D Cartesian geometry for documentation purposes, though our experience from comparing other accelerators in 2D and 3D says it should be similar. We would also like to investigate higher spatial order FEM.

REFERENCES

[1] M.L. Adams and E.W. Larsen, "Fast iterative methods for discrete-ordinates particle transport calculations," *Progress in Nuclear Energy*, vol. 40, no. 1, pp. 3–159, 2002.

[2] T. Bailey, "A piecewise linear finite element discretization of the diffusion equation," M.S. thesis, Texas A&M University, College Station, Texas, 2006.

[3] R.E. Alcouffe, "A stable diffusion synthetic acceleration method for neutron transport iterations," *Transactions American Nuclear Society*, vol. 23, pp. 203, 1976.

[4] T.A. Wareing, "Asymptotic diffusion accelerated discontinuous finite element methods for transport problems," Research Report LA-12425-T, Los Alamos National Laboratory Report, Los Alamos, NM, 1992.

[5] W.H. Reed, "The effectiveness of acceleration techniques for iterative methods in transport theory," *Nuclear Science and Engineering*, vol. 45, pp. 245, 1971.

[6] E.W. Larson, "Unconditionally stable diffusion synthetic acceleration methods for slab geometry discrete oridnates equations part 1: Theory," *Nuclear Science and Engineering*, vol. 82, pp. 47, 1982.

[7] J.S. Warsa, T.A. Wareing, and J.E. Morel, "Fully-consistent diffusion synthetic acceleration of linear discontinuous sn transport discretizations on unstructured tetrahedral meshes," *Nuclear Science and Engineering*, vol. 141, pp. 235–251, 2002.

[8] J.S. Warsa, T.A. Wareing, and J.E. Morel, "Krylov iterative methods and the degraded effectiveness of diffusion synthetic acceleration for multidimensional sn calculations in problems with material discontinuities," *Nuclear Science and Engineering*, vol. 147, pp. 218–248, 2004.

[9] Y.Y. Azmy, T.A. Wareing, and J.E. Morel, "Effect of material heterogeneity on the performance of dsa for even-parity sn methods," *Proc. ANS Topical Meeting, International Conference on Mathematics and Computation, Reactor Physics and Environmental Analysis*, vol. 1, pp. 55, September 27-30 1999.

[10] E.W. Larson, "A grey transport acceleration method for time-dependent radiative transfer problems," *Journal of Computational Physics*, vol. 78, pp. 459–480, 1988.

VITA

Name: Anthony Petru Barbu

Address:

Department of Nuclear Engineering

Texas A&M University

3133 TAMU

College Station, TX 77843-3133

Email Address: apbarbu@gmail.com

Education:

B.S., Nuclear Engineering, Texas A&M University, 2005

M.S., Nuclear Engineering, Texas A&M University, 2011